

# Modification of Polymer Surfaces with Respect to their Lubrication Properties

## **Dissertation zur Erlangung des Grades „Doktor der Naturwissenschaften“**

vorgelegt von

Marcus Heuberger

Rehovot, November 2001



An der  
Fakultät für Physik  
Universität Konstanz



In Zusammenarbeit mit dem  
Department of Materials & Interfaces  
Weizmann Institute of Science

Prof. Dr. G. Schatz

Prof. Dr. J. Klein



# TABLE OF CONTENTS

<b>1</b>	<b>EINFÜHRUNG</b> .....	<b>5</b>
<b>2</b>	<b>INTRODUCTION</b> .....	<b>9</b>
<b>3</b>	<b>MATERIALS &amp; METHODS</b> .....	<b>11</b>
3.1	MATERIALS .....	11
3.1.1	<i>Matrix Material</i> .....	11
3.1.2	<i>Linear Block Copolymer</i> .....	11
3.1.3	<i>Grafted PE-g-PEO</i> .....	13
3.2	SAMPLE PREPARATION.....	14
3.3	NUCLEAR REACTION ANALYSIS.....	17
3.4	SHEAR RESPONSE ANALYSIS.....	18
3.5	CONTACT ANGLE GONIOMETRY .....	23
3.6	SMALL ANGLE NEUTRON SCATTERING.....	24
3.7	OPTICAL PHASE INTERFERENCE MICROSCOPY .....	26
<b>4</b>	<b>MACRO- AND MICRO-PHASE SEPARATION IN POLYMER BLENDS</b> .....	<b>27</b>
4.1	THEORY .....	27
4.2	RESULTS .....	31
4.2.1	<i>SANS: Structural Analysis of Bulk Polymers</i> .....	31
4.2.2	<i>In Thin Films: Micro-phase Separated Domains Enhancing an Autophobic Effect of the Matrix-Film</i> .....	34
4.2.3	<i>NRA: Depth Distribution of Block Copolymer in Thin Films</i> .....	39
4.3	DISCUSSION .....	42
<b>5</b>	<b>FRICITIONAL PROPERTIES OF MODIFIED LDPE-SURFACES</b> .....	<b>45</b>
5.1	MODEL CALCULATIONS FOR BRUSHES IN DIFFERENT SOLVENT CONDITIONS .....	45
5.2	RESULTS .....	48
5.2.1	<i>Polymer and Modified Polymer Sheared against Mica</i> .....	49
5.2.2	<i>Polymer and Modified Polymer Sheared against CTAB on Mica</i> .....	53
5.2.3	<i>Overview of the Frictional Modification of the Systems Investigated</i> .....	55
5.3	DISCUSSION .....	57
<b>6</b>	<b>CONCLUSIONS &amp; OUTLOOK</b> .....	<b>59</b>
<b>7</b>	<b>BIBLIOGRAPHY</b> .....	<b>61</b>

## TABLE OF CONTENTS

# 1 Einführung

Künstliche Polymere stellen eine faszinierende Materialgruppe dar. Sie können aus wenigen Monomeren bis hin zu langen Polymerketten modelliert werden. Durch Variation der Anzahl und Zusammensetzung der Monomere kann man Festkörper- und Materialeigenschaften kontrollieren, so dass Löslichkeiten und Viskositäten variiert werden können. Eine Variation der Festkörpereigenschaften ist auch möglich durch das Mischen zweier oder mehrerer Homopolymere. Wegen der hohen, ungünstigen Wechselwirkungsenergien zwischen den einzelnen Homopolymeren in Verbindung mit der geringen translatorischen Entropie aufgrund der großen Molekulargewichte können normalerweise keine stabilen Mischungen gebildet werden, daher müssen sie oft durch sogenannte Blockkopolymere stabilisiert werden. Diese Blockkopolymere besitzen die Eigenschaften eines jeden in der Mischung verwendeten Homopolymers als Blöcke, die chemisch fest miteinander verbunden sind. Die Stabilität, die Elastizität und auch die Härte können mit diesen Blockkopolymeren auf die gewünschten Werte gebracht werden [1-5]. Polymere mit ihren verschiedenen positiven Eigenschaften sind aus unserem täglichen Leben nicht mehr wegzudenken. Man findet sie heutzutage für alle möglichen Verwendungszwecke, sei es bei kommerziellen, technologischen oder medizinischen Anwendungen.

Während die Festkörpereigenschaften für eine Vielzahl von Verwendungszwecken von Bedeutung sind, so spielen doch die Oberflächeneigenschaften durch ihre Wechselwirkungen mit der Umgebung die entscheidende Rolle. Zusätzlich zu den Materialeigenschaften sind daher die Kompatibilität oder Inkompatibilität (hydrophobisch oder hydrophilisch) an der Oberfläche als Wechselwirkung mit der Umgebung von entscheidender Bedeutung. Wichtig ist auch die Auseinandersetzung mit den Adhäsions- und Reibungseigenschaften und die Möglichkeit, maßgeschneiderte Polymeroberflächen herzustellen, offeriert eine Vielfalt an Lösungsmöglichkeiten für die unterschiedlichsten Systeme. Die Möglichkeit, Materialien nach ihren Festkörpereigenschaften zu verwenden und zugleich die Oberflächen entsprechend ihrer Wechselwirkungen mit der Umwelt anzupassen, bedeutet für die Entwicklung von neuen, anspruchsvollen Materialien eine große Herausforderung. In den künstlichen Polymersystemen versucht man, sich auch von der Natur inspirieren zu lassen. Diese biologischen Systeme haben im Laufe der Jahrtausende die besten Entwicklungen hervorgebracht und haben sie in fast jedem Detail bis zur Perfektion verfeinert.

Das Forschungsziel, das innerhalb dieser Arbeit verfolgt wird, ist die Entwicklung einer selbstaufbauenden Oberfläche, die sich spontan aus einem Reservoir im Festkörper bildet und die damit auch selbstregenerierende Eigenschaften besitzt, um von Außen zugefügte Schäden auszugleichen. Daher wurden keine Methoden verwandt, die auf einer einmaligen chemischen Ätzung oder auf einem

physikalischen Ionenbeschuß beruhen [6-8]. Es konnte auch nicht das Ziel sein, die Oberfläche mit Hilfe eines zusätzlichen Polymers einmalig zu überziehen.

Bei Untersuchungen von natürlichen biologischen Systemen, in denen es auf exzellente Gleiteigenschaften ankommt, um die Reibung und den Verschleiß zu reduzieren, fand man lange Polymermoleküle. Diese Polymermoleküle findet man zum Beispiel in Säugetiergelenken, in der Tränenflüssigkeit oder im Blut [9-14]. Diese langen Moleküle sind Glycosaminoglycane und deren Untergruppe die hygroskopischen, und in Wasser stark anschwellenden Hyaluronsäuren. Ihre speziellen reibungsreduzierenden Eigenschaften in Synovialflüssigkeit (Gelenkflüssigkeit) oder im Blut sind noch nicht vollständig geklärt. Das Auftauchen dieser Moleküle in allen Bereichen, in denen es auf geringe Reibung ankommt, lässt jedoch darauf schließen, dass diese langkettigen und weitverzweigten Moleküle einen entscheidenden Beitrag zu den Gleiteigenschaften liefern.

Die Untersuchung von Modellsystemen hinsichtlich ihrer Reibungseigenschaften, wie zum Beispiel lange Polymerketten, die permanent an eine feste Unterlage gebunden sind (sogenannte Polymerbürsten), deuteten in die gleiche, reibungsreduzierende Richtung. Auch in diesen Systemen verbesserten die Polymerketten die Gleiteigenschaften deutlich und konnten wesentlich höhere Normalkräfte aufnehmen als monomerische Gleitmittel. Während monomerische Gleitmittel schon bei geringen Normaldrücken zwischen atomar glatten Glimmeroberflächen fest wurden und damit Scherkräfte angelegt werden konnten [15-19], konnten bei wesentlich höheren Normaldrücken zwischen den mit Polymerbürsten überzogenen Glimmeroberflächen nur Scherkräfte angelegt werden, die unterhalb des Auflösungsereichs der Oberflächenkraftmaschine lagen ( $< 100$  nN) [20-25]. Die reibungsverbessernden Eigenschaften von Polymeren, die die harten Glimmeroberflächen überziehen, liegt in ihrer Fähigkeit begründet, hohe Normalkräfte aufnehmen zu können, sich aber nicht zu überlappen und zu verhaken. Damit ist gewährleistet, dass immer eine Flüssigkeitsschicht zwischen den gescherten Oberflächen erhalten bleibt und damit die Reibung reduziert wird.

Das Ziel dieser Arbeit war es, sowohl die Erkenntnisse aus den Modellsystemen als auch aus den biologischen Beobachtungen zusammenzuführen. Diese Erkenntnisse sollten dazu dienen, die Grenzflächeneigenschaften eines Systems zu verbessern, das von praktischer Bedeutung ist. Es handelt sich dabei um das Polyäthylen, das zur Zeit noch ohne Oberflächenmodifizierung für künstliche Gelenkimplantate verwendet wird [26-28].

Dabei wurden sowohl die oberflächenbezogenen Phänomene als auch die phasenbezogenen Eigenschaften im Festkörper betrachtet, die daraus resultierten, dass verschiedene Additive in das Homopolymer eingebracht wurden. Im ersten Teil wird das Verhalten eines linearen Blockkopolymer-Homopolymer Gemisches behandelt. Im zweiten Teil werden Untersuchungen eines aufgepfropften Blockkopolymers beschrieben, das in einen Matrixfilm eingebracht wurde. Die Messungen haben gezeigt, dass die Gleitwirkung in den modifizierten Systemen im Vergleich zu den nichtmodifizierten Filmen um eine Größenordnung verbessert werden konnte.

Die Untersuchungen zu den Strukturen und die Tiefenprofilmessungen wurden mit Neutronenkleinwinkelstreuung und nicht-resonanter Kernreaktionsanalyse durchgeführt. Zur Charakterisierung der Oberflächeneigenschaften wurden

hauptsächlich optische Phaseninterferenz-Mikroskopie, Kraftmikroskopie und Kontaktwinkelmessungen verwendet. Um die Gleiteigenschaften der modifizierten und nichtmodifizierten Polymeroberflächen zu untersuchen, wurde eine Oberflächenkraftmaschine entsprechend den gewünschten Auflösungseigenschaften modifiziert.

Aus den Erkenntnissen des zweiten Teils können allgemeine Voraussetzungen für gleitverbessernde Oberflächenbeschichtungen abgeleitet werden. Weitergehende Studien können zu einem Wissenstransfer zu nicht biologischen Systemen führen. Zum Beispiel können die gewonnenen Erkenntnisse auf das Beschichten von Lagerschalen oder Computerfestplatten und Leseköpfen übertragen werden.



## 2 Introduction

Artificial polymers are a fascinating group of materials purpose-designed from a few monomers to long polymer chains. Control over the bulk properties is readily achieved by varying the amounts and compositions of the monomers (solubility and viscosity can be varied). Control over bulk properties is also possible by blending two or more homopolymers. Homopolymers generally do not form stable blends because of the high unfavourable interaction energies together with the low translational entropy due to the large molecular size. Therefore, a block copolymer is often used to improve the compatibility, the resultant material having the properties of each homopolymer in blocks that are chemically attached to each other. With the latter the stability, elasticity and toughness can be tuned to the desired values [1-5]. Polymers are found in various commercial, technological or medical applications depending on their different properties and thus are playing an important role in our daily life.

Materials for specific applications are often chosen according to their bulk properties. However, they interact with the surrounding via their surfaces. Thus, interfacial compatibility or incompatibility (hydrophobic, hydrophilic) can determine the suitability of the materials. Issues of adhesion and lubrication are important and the ability to design polymeric interfaces offers a large variety of tailor-made solutions for different systems. The ability of using materials according to their bulk needs and at the same time to model the surfaces according to the special purposes for the outer world is an important issue in material technology. In synthetic polymeric systems, one tries as well to learn from nature, where evolution has frequently led to the development of optimal solutions.

The aim of the research described in this thesis is to design a surface layer, with the ability to spontaneously form from a bulk reservoir and with the possibility of self-healing or recovering from damage. Therefore, no methods were utilised such as chemical etching, physical ion-bombardment or corona treatment [6-8]. It was also not the aim to make use of surface coating using different polymer as mounted top layer.

Investigations into the properties of natural systems where excellent lubrication is necessary to reduce friction and wear, confirmed the presence of long chained polymeric molecules. Examples of such systems include the blood flow, the cornea of the eye and the mammalian joints [9-14]. These molecules are the glycosaminoglycans and among those the hygroscopic and in water strongly swelling hyaluronic acids (HA). The functional role of these polymers is not yet fully understood in the environments of the synovial fluid or in the blood. However, their appearance in all these systems where low friction is required gives rise to the idea that long chained molecules can affect the lubricating properties.

Previous studies of friction in model systems, for example polymer chains permanently attached to a hard surface and their lubrication enhancing behaviour, showed the same effect. In addition, here the polymer chains enhanced the lubricating properties dramatically relative to monomeric lubricants. The monomeric lubricants

were squeezed down to a few monolayers and solidified already at low pressures between atomically smooth mica surfaces and a yield stress was required for sliding [15-19]. At quite high pressures between the polymer-brush-coated mica surfaces, the surfaces on sliding experienced a shear response that was lower than the resolution of the surface force balance ( $< 100$  nN) [20-25]. The lubricating effect of polymers end-attached to a surface occurs because such polymer chains can support a large normal load while maintaining a very fluid interface due to very weak mutual interpenetration.

The aim of this work is to utilise and combine the knowledge gained in the study of model systems and the inspiration from biological systems for the investigation of the interfacial properties of a new type of system, polymer surfaces exposing a self assembled polymeric surfactant. An analogous system, polyethylene, though with no surface coating, is used for artificial body implants in synovial joints [26-28].

The thesis deals with surface-related phenomena and bulk phase behaviour that originate from the incorporation of different additives into the initial homopolymer. In the first section, the behaviour of a linear block copolymer-homopolymer blend was examined. In the second part, properties of a grafted block copolymer incorporated into the matrix film were investigated. It was found that the lubrication was enhanced by almost one order of magnitude. From the findings of the second part it is also possible to gain a general understanding of the nature of polymers that lead to lubrication-enhancing surface coatings. Further studies can lead to a transfer of this knowledge to other systems, for instance coatings for bearings in engines or computer hard discs.

The main structural and depth-profiling experimental investigations were carried out using small angle neutron scattering and nuclear reaction analysis. The characterisations of the surface properties were performed mainly with optical phase interference microscopy, atomic force microscopy and contact angle measurements. To examine the friction between the sheared modified and non-modified polymer surfaces a surface force balance was used and modified according to the purposes.

## 3 Materials & Methods

### 3.1 Materials

In the following section the polymeric materials used for the experiments are described in detail. Polished silicon wafers (Institute of Electronic Materials Technology, Warsaw, Poland) or microscopy glass slides served as substrates.

#### 3.1.1 Matrix Material

The matrix polyolefins that were used as a carrier for modifying materials were either low-density poly[ethylene] (LDPE) or poly[ethylene-*co*-propylene] (PEP) kindly donated by D. J. Lohse and J. Allgaier, respectively. The molecular weight of the LDPE was  $M_w = 148$  kg/mol with a polydispersity of  $M_w/M_n = 7.6$ . The PEP had a molecular weight of  $M_w = 90$  kg/mol.

#### 3.1.2 Linear Block Copolymer

Block copolymers were synthesised via living anionic polymerisation. This well-characterised method for the synthesis of block copolymers results in narrow molecular weight distribution and well-defined block structure [29]. The principles for the polymerisation of poly[ethylene-*co*-propylene-*b*-(ethylene oxide)] (PEP-*b*-PEO) were described by Allgaier *et al.* [30] or of poly[butadiene-*b*-(ethylene oxide)] (PBD-*b*-PEO) by Förster and Krämer [31]. In the following paragraphs the polymerisation of the linear block copolymer poly[ethylene-*b*-(ethylene oxide)] (PE-*b*-PEO) is described. It was carried out in a similar two-step procedure under the supervision of J. Allgaier at the Forschungszentrum Jülich, Germany (*Figure 3-1*).

##### Solvents and Monomers for PE-*b*-PEO

Benzene (Merck) was first purified in high vacuum ( $10^{-3}$  mbar) for the purpose of removing the oxygen solved in the solvent and then distilled onto butyl lithium. The butyl lithium was then allowed to react for 12 h—while stirring—with impurities in the solvent. Tetrahydrofuran (THF, Merck) was purified by distilling from sodium in order to dry it from  $H_2O$  remains. The butadiene was purified by treatment with dibutylmagnesium, and then distilled onto n-butyl lithium. Ethylene-oxide (EO) (Fluka) was distilled onto n-butyl lithium and allowed to purify for 2 days. Thereafter it was stirred on  $CaH_2$  for 12 h before being transferred into ampoules. The deuterated EO was purified and dried twice in a similar manner on  $CaH_2$  before usage.

##### Polymerisation of Precursor PBD-OH and PE-*b*-PEO

All manipulations were performed under high vacuum of  $10^{-3}$  mbar in glass reactors, provided with break seals for the administration of different reagents. Living

butadiene was prepared in good solvent conditions in benzene with *sec*-butyl lithium as initiator. The synthesising process is described in *Figure 3-1*.

The polymerisation to PBD–Li<sup>+</sup> was allowed to proceed for 24 h. The PBD–OH was formed by reacting the living PBD–Li<sup>+</sup> first with EO in a many-fold excess over the initiator concentration, this mixture was stirred for 12 h and terminated with acetic acid to form lithium acetate that could be separated from the polymer PBD–OH in solution. The polymer was precipitated in analytical grade methanol (Sigma). PE–OH was obtained by hydrogenation of PBD–OH in solution with heptane in the presence of a Pd/BaSO<sub>4</sub> catalyst (Aldrich). The process was allowed to proceed for 12 h at a pressure of 45 bar and a temperature of 100 °C.

The PE–OH was precipitated in a mixture of methanol and acetone (50:50), followed by filtering the solved polymer through a glass filter for the purification of the polymer from the catalyst. The polymer was then dried under reduced pressure of the high vacuum line at a temperature of 110 °C for 5 days to remove the entire methanol, which would act as a possible initiator for EO homopolymer.

In the next stage of the process the PEO block was formed. The polymer PE–OH was dissolved in dry THF at a temperature of 70 °C. These manipulations were performed under high-vacuum conditions without allowing the polymer to come into contact with air. To create the living polymer PE–OH<sup>–</sup>K<sup>+</sup>, the polymer solution was titrated with cumylpotassium. The solution is then a deep red-colour and acts as a marker for the reaction. Addition of cumylpotassium was stopped after a slight orange colour in the polymer solution persisted for 5 minutes. After the mixture was stirred for ½ h the colour disappeared completely. Excess THF for the following polymerisation and the deuterated EO were added, after which the deuterated EO was allowed to polymerise at 75 °C for 3 days. Reactions were terminated with acetic acid.

At –10 °C the product PE–*b*–PEO was precipitated first in acetone and second in heptane and centrifuged after each precipitation step. The final cleaning and drying were performed by solving in benzene and freeze drying in liquid N<sub>2</sub>, sublimation of the benzene and then drying under reduced pressure at the high-vacuum line.

The polydispersity determined by gel phase chromatography (GPC) of the precursor polymer PE–OH is  $M_w/M_n = 1.025$  and  $M_n = 5179$  g/mol. According to H-NMR the content of the deuterated PEO block in the PE–*b*–PEO copolymer was 72.3 % whereas the <sup>13</sup>C-NMR measurements showed a content of 73.2 % in very good agreement. This results in a calculated molecular weight average for the PEO-chain of  $M_n = 13827$  g/mol. The specifications of the polymers are given in *Table 3-1*.

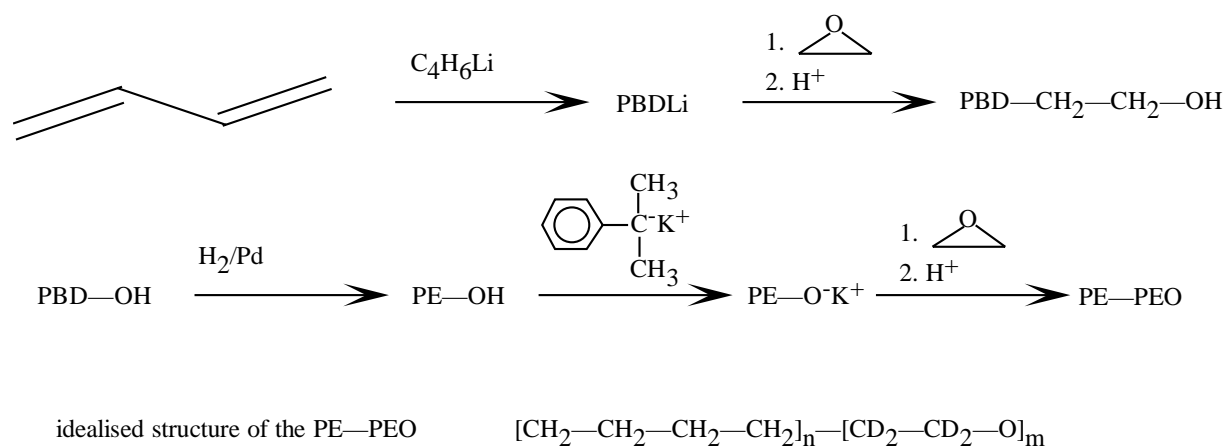


**Figure 3-1:** Sketch of the two-step anionic polymerisation of the block copolymer poly[ethylene-*b*-(ethylene oxide)] (PE-*b*-PEO). First poly[butadiene] (PB) as precursor block is polymerised from a lithium initiator and finalised with ethylene oxide. Then hydrogenation of PB to poly[ethylene] (PE) is done with a catalyst under high pressure. Finally the second block deuterated poly[ethylene oxide] is polymerised after reaction of the first block with a potassium initiator.

The PEP-*b*-PEO was synthesised following the procedure in section 3.1.2 and used in the configurations listed in *Table 3-1*. Precursor block polymer for the PEP was a polyisoprene-OH—instead of the PBD-OH for PE-OH—that was hydrogenated or deuterated, depending on the purpose of the investigations. The block copolymer was kindly donated by J. Allgaier, Forschungszentrum Jülich, Germany.

### 3.1.3 Grafted PE-*g*-PEO

The grafted block copolymers (*Figure 3-2*) were synthesised and kindly donated by Å. Halldén, Lund University, Sweden. A PE backbone with acrylic acid (AA) side groups esterifies with monomethyl ether end modified PEO (MPEO) homopolymer in various block lengths at a temperature of 140 °C in *o*-xylene [32]. Upon completion of the reaction the AA side groups, were esterified by methanol. While cooling the PE-*g*-PEO precipitated whereas the excess MPEO stayed in solution and was decanted from the swollen PE-*g*-PEO. The PE-*g*-PEO was cleaned from MPEO while stirring and decanting from cold methanol. This treatment was repeated until no remains of MPEO-homopolymer were monitored in the decanted methanol with FT-IR spectroscopy. The PE-*g*-PEO was then dried under vacuum at room temperature.

The weight percent of the side blocks MPEO was 30 and 45 % for the PE-*g*-PEO750 and PE-*g*-PEO2000 respectively where the number indicates the molecular weight of the PEO side chains.

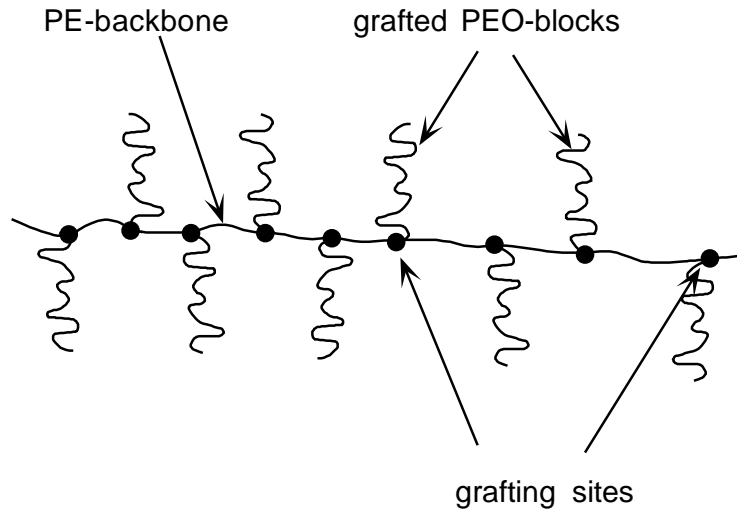


**Figure 3-2:** Schematic drawing of the grafted block copolymer PE-g-PEO.

Label of the block copolymer	precursor/backbone $M_n$ [g/mol]	precursor/backbone $M_w/M_n$	Block copolymer $M_n$ [g/mol]	$M_w/M_n$ diblock
<i>d</i> PEP5- <i>b</i> -PEO5	4750	1.03	10650	1.03
<i>d</i> PEP5- <i>b</i> -PEO15	4770	1.03	20800	1.03
PE5- <i>b</i> - <i>d</i> PEO14	5180	1.03	Calculated 19000	
PE-g-PEO750	16000		750	
PE-g-PEO2000	16000		2000	

**Table 3-1:** The different block copolymer configurations used for the experiments. *d* indicates the block that is partially or fully deuterated for nuclear reaction analysis. *b* or *g* shows the way the block copolymer is formed either as linear block or as grafted block respectively.

## 3.2 Sample Preparation

### 1) Preparation of thin films

Thin polymer films in the range of 200 nanometers to 600 nanometers were prepared by spin coating. The thickness was controlled by the concentration and thus the viscosity of the solution and the spinning rate of the spin-coater. The PEP films were spin coated at room temperature from toluene solution on native silicon wafers with a size of about one cm<sup>2</sup>. PEP films containing PEP-*b*-PEO block copolymer were spin coated on freshly cleaved mica and then transferred immediately on top of an ion beam cross-linked PEP film via a special jig as shown in *Figure 3-3* and earlier described in [33].

LDPE films were prepared on top of etched silicon wafers. Native oxide layer were first removed in an aqueous solution of hydrofluoric acid (4 %, Fluka). The films were then spin coated at a temperature of 140 °C from tetradecane (Fluka). LDPE films had a roughness (RMS) value of 0.5 nm measured by optical phase interference microscopy over the whole sample size.

The Si-wafer including the thin films were annealed in ampoules under

different conditions for various periods and temperatures. Conditions for the films were either 1) reduced pressure of  $10^{-4}$  mbar, 2) incorporating a spin coated or solvent cast layers of homopolymer PEO on top of the films of different molecular weights at the same reduced pressure or 3) the films were in contact with a humid atmosphere or with bulk water within the ampoules.

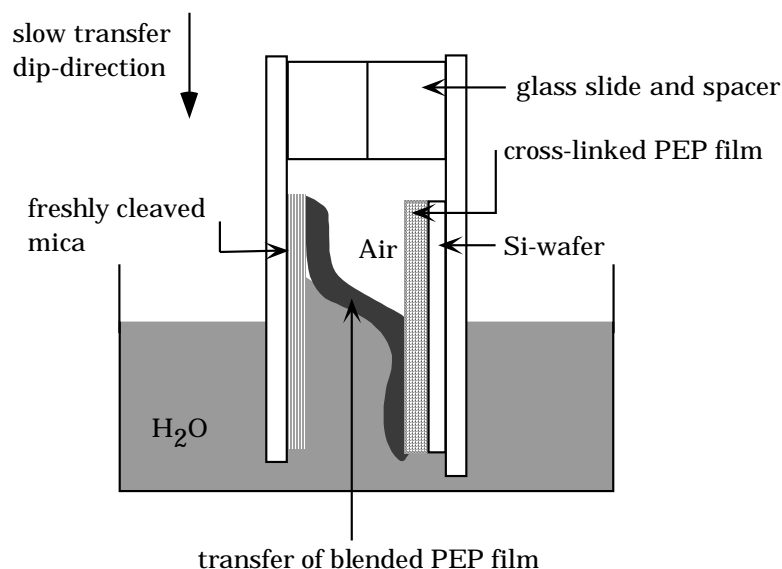


**Figure 3-3:** Schematic diagram of the transfer of a PEP film containing PEP-*b*-PEO spin coated on mica (left) and transferred onto a PEP film spin coated on silicon (right). The PEP films were cross-linked in a  $^3\text{He}$  ion beam for various periods.

## 2) Preparation of films with intermediate thicknesses

Films in the intermediate thickness range of about 50 – 70 micrometers were solvent cast on glass slides by depositing a layer of the polymer solution onto the slide and letting the solvent evaporate. Polymer blends of LDPE with grafted block copolymers were cast from *o*-xylene solution on glass surfaces at a temperature of 110 °C. The glass slides were cleaned by using ( $\text{H}_2\text{O}_2:\text{H}_2\text{SO}_4$ )-solution ( $\frac{1}{3}:\frac{2}{3}$ ). Following the casting, the films were annealed at a temperature of 110 °C for 48 hours to ensure slow evaporation of the solvent and complete drying of the film. For further smoothing, the films were pressed between two glass slides at 130 °C. *Figure 3-4* shows the effect of pressing the surfaces. The surface shown in *a*) before pressing had a roughness (RMS) value of 15 nm measured by AFM over the whole sample size shown below and a pattern characteristic of lamellar formation; whereas *b*) showed a smoothed surface with an RMS value of 2 nm related as well to the whole sample size. Film thicknesses of about 20 – 30  $\mu\text{m}$  were achieved by this method.

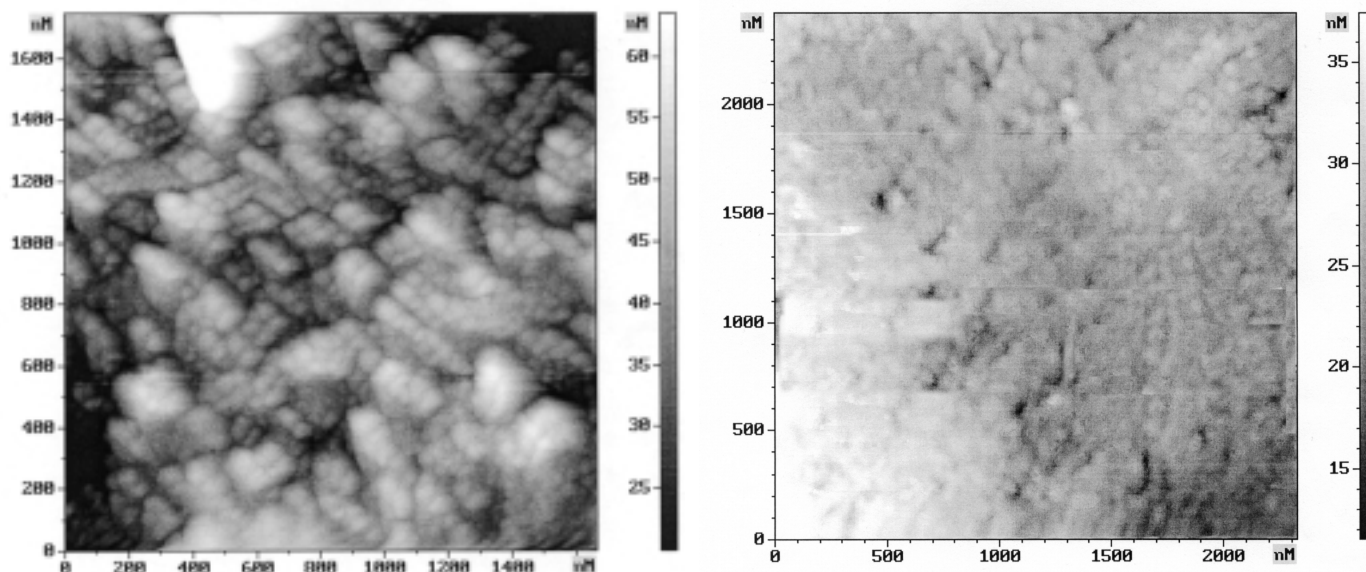


**Figure 3-4:** Two AFM scans of the as-solvent-cast film (a) with RMS value of 15 nm and of the pressed surface (b) with RMS value of 2 nm related to the whole sample size.

For shear response analysis (SRA), the films were glued with their former air facing side onto opposing crossed cylindrical quartz lenses (radius 1 cm) using the resin Epon 1004F™. Either hydrophilic freshly cleaved mica surfaces or mica previously coated with adsorbed cetyl-trimethyl-ammonium-bromide (CTAB) were used as the surface opposite the LDPE film. CTAB is a short chain hydrocarbon leading to a hydrophobic surface. The coating was performed according to the technique described by Gee [34]. The monolayers were deposited onto the mica by adsorption from solution. This was achieved by submerging the mica into a solution (concentration of  $5 \times 10^{-4} \text{ mol/dm}^{-3}$  which is below the c. m. c.) of the surfactant for 30 min. After this time the mica was rinsed with conductivity water to remove excess of CTAB. The monolayer was considered to be adsorbed onto the mica when on retraction of the CTAB-coated mica from the water, the water did not wet the surface. Surfaces were characterised using AFM by Patrick and Sterthaus [35,36]. CTAB on mica films showed spherical micelles forming on top of these films as blobs.

### 3) Preparation of bulk samples

Samples for Small Angle Neutron Scattering (SANS) were prepared by dissolving the components in toluene at block copolymer concentration of 0.5 %, 1 %, 2 % in the homopolymer and as well undiluted block copolymer. The blends were dried under high vacuum at temperatures of 50 °C. The dry blends were transferred under an argon atmosphere in a quartz cell used for small angle neutron scattering at 150 °C. Samples were cooled down to room temperature at a rate of 20 °C/h. The thickness of the polymer layer was about 1 mm.

### 3.3 Nuclear Reaction Analysis

Nuclear reaction analysis (NRA) is a non-resonant direct depth profiling technique which has been extensively used over the past decade to investigate distributions of deuterated polymeric species embedded in a hydrogenated matrix [37-39].

The investigation is based on the nuclear reaction  ${}^2\text{H}({}^3\text{He}, {}^4\text{He}){}^1\text{H}$  and the energy loss of the reaction products while passing through matter [40].

*Figure 3-5* shows the experimental set-up for  $\alpha$ -particle detection mode. The collimated mono-energetic  ${}^3\text{He}$ -ion-beam—with an incident energy of  $E_0({}^3\text{He}) = 1,2$  MeV in our case—reacts with the deuterium-labelled polymeric sample in different depths. The reaction  ${}^2\text{H}({}^3\text{He}, {}^4\text{He}){}^1\text{H}$  has the maximal cross section of 900 mbarn at incoming  ${}^3\text{He}$  energy of 650 keV [41]. The Q-value of the reaction is with 18.352 MeV sufficiently high for the emerging reaction products to be distinguished from background noise. To suppress elastically scattered  ${}^3\text{He}$ -ions which might saturate the detectors and the electronics with pile-up counts a magnet and a slit system is placed in front of the detector.

In our case the  $\alpha$ -particles were detected in forward direction under an angle  $\theta$  of  $30^\circ$  to the incident beam in a semiconductor detector (Canberra PD 100-13-100 AM PIPS detector), recorded in a multichannel analyser and read out from a PC.

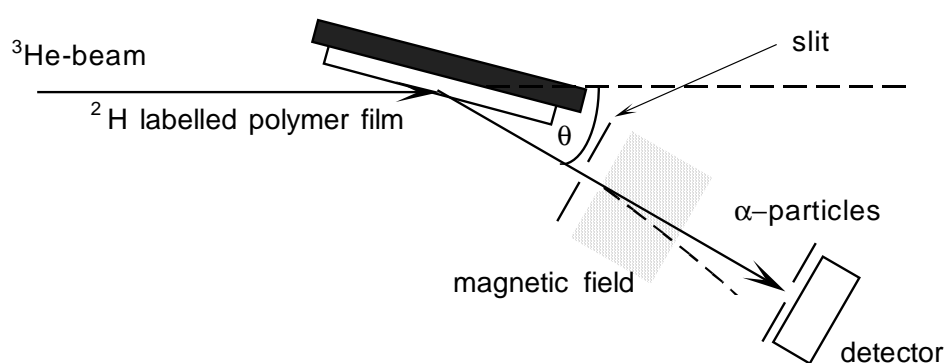


**Figure 3-5:** A schematic diagram of the slits and magnet positions for the detection of alpha particles emerging from a polymeric sample after undergoing the nuclear reaction  ${}^2\text{H}({}^3\text{He}, {}^4\text{He}){}^1\text{H}$ .

The incident  ${}^3\text{He}$  particles lose energy by inelastic electronic scattering in the sample and the reaction probability is reduced with increasing depth. The  $\alpha$ -particles created in the reaction again lose energy while passing through the sample until they reach the surface.

Energy of the particles reaching the detector is then a measure of the depth  $x$  at which the nuclear reaction occurred, while their abundance at that energy is a measure of the deuterium concentration at  $x$ . This information then yields the  $c(x)$  depth profiles.

Energy spectra from the multichannel analyser of the  $\alpha$ -particles are converted to the depth distribution of the deuterated species in the polymeric samples. This is

achieved by normalising the measured spectra with the experimentally measured reaction cross-section, and the use of the Ziegler tables [42-45].

### 3.4 Shear Response Analysis

The principle of shear response analysis (SRA) is as follows: a known lateral motion  $\Delta x_0$  is applied to one of two surfaces that are in contact under a load  $F$ , which is attached to a shear-force-measuring spring (spring constant  $k_s$ ) as indicated in *Figure 3-6*. Any shear or frictional force between the surfaces bends the spring by  $\Delta x$ , so that the actual motion of the top surface is  $(\Delta x_0 - \Delta x)$  and is measured. This yields the frictional or shear force  $k_s \Delta x$  at the load  $F$ .

Depending on the normal load, the medium between the surfaces and the surfaces themselves, differences in the frictional properties can be detected and can give insight in the frictional behaviour of materials and lubricants. The measurements were carried out at room temperature.

The detailed implementation is carried out using a modified Surface Force Balance (SFB) as the base for the SRA, *Figure 3-6*. Two cylindrical lenses with a radius of 0.01 m are mounted in a crossed configuration. The upper lens is attached to two vertical leaf springs that are screwed to a micrometer carriage and can be moved horizontally, whereas the lower one is supported by two horizontal leaf springs (for simplicity in the scheme only one is shown) in a bath and can be moved only in vertical direction in single steps S1 by a stepper motor. The distance  $(\Delta x_0 - \Delta x)$  that the top lens moves horizontally is monitored by a change in the voltage of an air gap capacitor. At large separation of the surfaces where there is no frictional force so that  $\Delta x = 0$ , the air gap capacitor shows equidistant differences in voltage for equal steps in the applied motion  $\Delta x_0$  (within the noise level due to for example building vibrations) and can be calibrated accordingly. The load increase in contact per S1 step was derived from the knowledge of the horizontal spring constant and the measurement at large surface separations of the step size S1 via Fabry-Perot-interferometry, the optical distance measurement used in the classic SFB experiments. When the surfaces come into contact, the noise level is significantly reduced and depending on the shear forces between the two surfaces the distances  $(\Delta x_0 - \Delta x)$  moved in the air gap capacitor are reduced (by  $\Delta x$ ) compared to the calibration measurement  $(\Delta x_0)$ , i.e. a finite friction force  $k_s \Delta x$  becomes measurable. The point where the noise level reduction first occurred defines the zero load measurement.

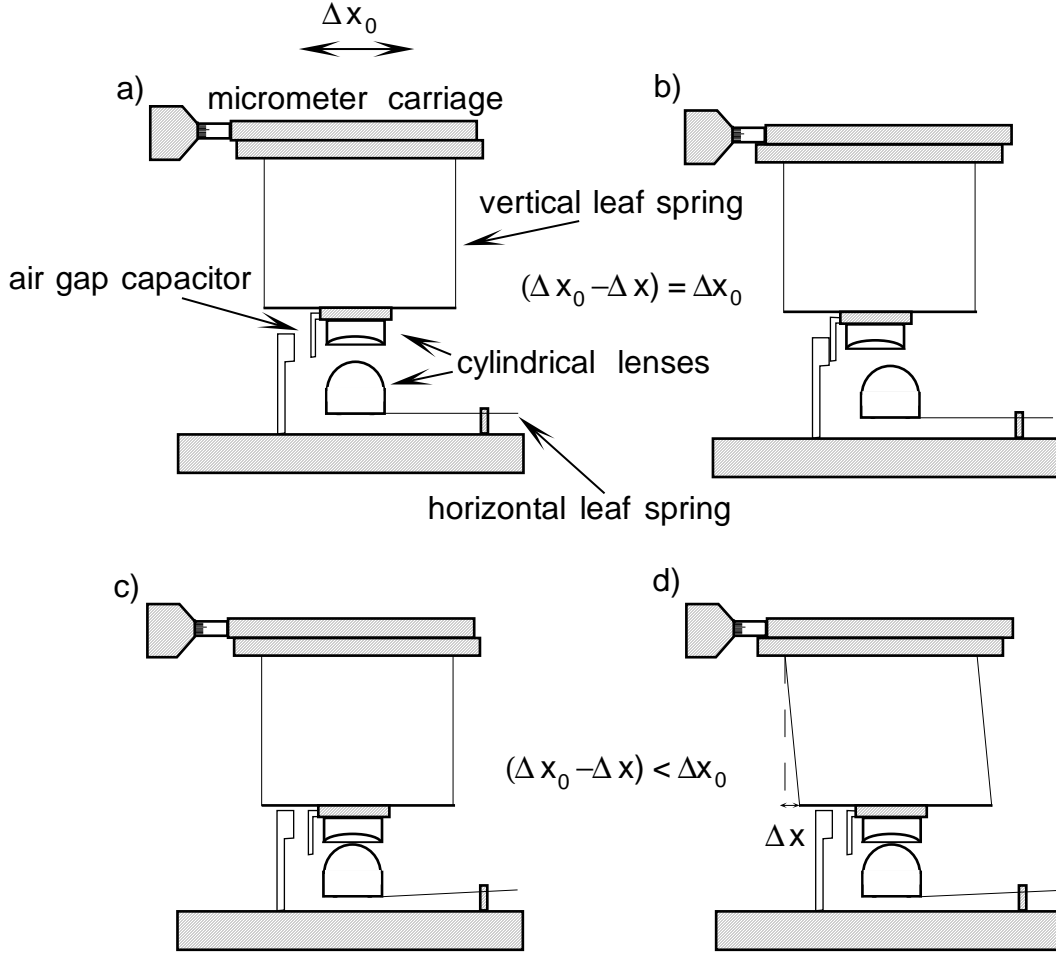


**Figure 3-6:** A schematic drawing of the shear response analysis apparatus. In a) and b) the SRA is in friction free mode for calibration of the air gap capacitor; moving the micrometer carriage by  $\Delta x_0$  only reduces or enlarges the distance in the air gap capacitor by the same amount. In c) and d) the surfaces of the lenses in the SRA-apparatus are in contact; c) shows a sketch for normal load but no shear force applied whereas in d) the applied shear force leads to a bending of the shear springs by  $\Delta x$  and a reduction of the distance in the air gap capacitor by  $(\Delta x_0 - \Delta x)$  which is smaller than  $\Delta x_0$ .

With the knowledge of the vertical spring constants, the applied and the response shear force can be plotted.

$$\Delta F_{s\_response} = k_s (\Delta x_0 - (\Delta x_0 - \Delta x)) = k_s \Delta x \quad (3.1)$$

Henceforth the total shear force is

$$F_{s\_response} = \sum \Delta F_{s\_response} \quad (3.2)$$

where  $F_{s\_response}$  is the total shear force,  $\Delta F_{s\_response}$  the shear force per lateral movement step applied in the micrometer carriage,  $k_s$  is the spring constant of the

vertical springs,  $\Delta x_0$  are the distances applied in the micrometer carriage,  $\Delta x$  are the distances moved of the sliding surfaces.

The applied motion can be written as  $F_{applied} = \sum \Delta x_0$  and therefore in the limit of rigid contact (no sliding)  $F_{s,response} = F_{applied}$ .

Typical curves of  $F_{s,response}$  and  $F_{applied}$  are shown in *Figure 3-7* where the main graph shows a measurement with response, i.e. the surfaces are in contact, whereas the inset shows a calibration measurement with a large separation between the two surfaces.

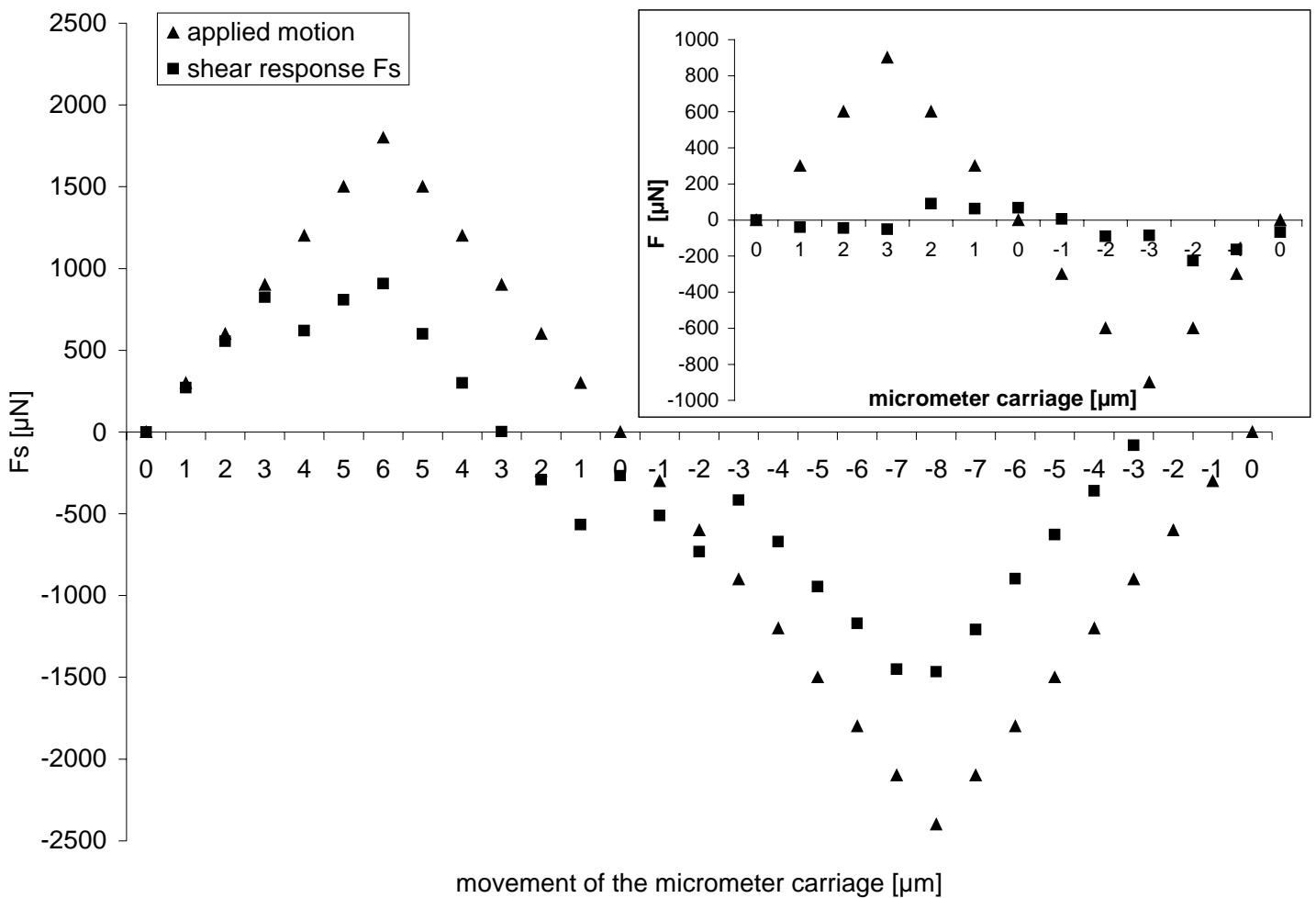


**Figure 3-7:** A shear response curve where the triangles show the applied force via the micrometer carriage and the squares show the response in the air gap capacitor. Inset: a typical calibration curve for the—large separation case—theoretically applied force in the micrometer carriage (triangles) and the shear response measured in the air gap capacitor (squares). The deviation from zero shear response is due to noise arising from the building vibrations.

The shear force  $F_s$  is represented in terms of the second moment.

$$\sigma(F_s) = \sqrt{\frac{n \sum F_s^2 - (\sum F_s)^2}{n(n-1)}} \quad (3.3)$$

where  $F_s$  is the shear force and  $n$  are the measured steps  $\Delta x_0$  in the micrometer carriage with the respective normal force.

*Figure 3-8* shows a plot of  $\sigma(F_s)$ , against the applied normal load  $F_n$  normalised to the radius of curvature  $R$ . The standard errors are plotted in direction of the normal load  $F_n$  as measured in a separate experiment at large surface separations with Fabry-Perot interferometry of the SFB. This standard error is valid for all the measurements but plotted only once for clarity (open triangles in *Figure 3-8*). The systematic error for the first contact of the two surfaces is one step in S1. The errors marked in y-direction are the standard errors derived from the calibration measurements of  $\Delta x_0$  in large separation of the two later compressed and sheared surfaces.

In *Figure 3-8*, typical graphs of a measurement are presented for two different sheared surfaces. The  $F_s$  value at the negative normal load reflects the calibration measurement with large surface separations. In the first case (LDPE sheared against CTAB coated mica in air; open triangles) as soon as the top-surface was made to move there was a laterally measurable shear response between the two surfaces in contact ( $(\Delta x_0 - \Delta x) < \Delta x_0$ ), which is expressed as an increase of the value of the standard deviation of  $F_{s, response}$ . The earlier the response was measurable and the steeper the slope of the increase, the higher the friction between the two surfaces.

The second case (LDPE sheared against CTAB-coated mica in ethanol; open squares), moving the micrometer carriage by  $\Delta x_0$  caused no measurable shear response  $\Delta x$ . Until a compression of about 300 mN/m was applied. This was the so-called low response region. Then an increase in the response in  $F_{s, response}$  and correspondingly in the  $\sigma$  of  $F_{s, response}$  could be seen. Continuing with further compression of the two surfaces led to a slope almost the same as in the first case.

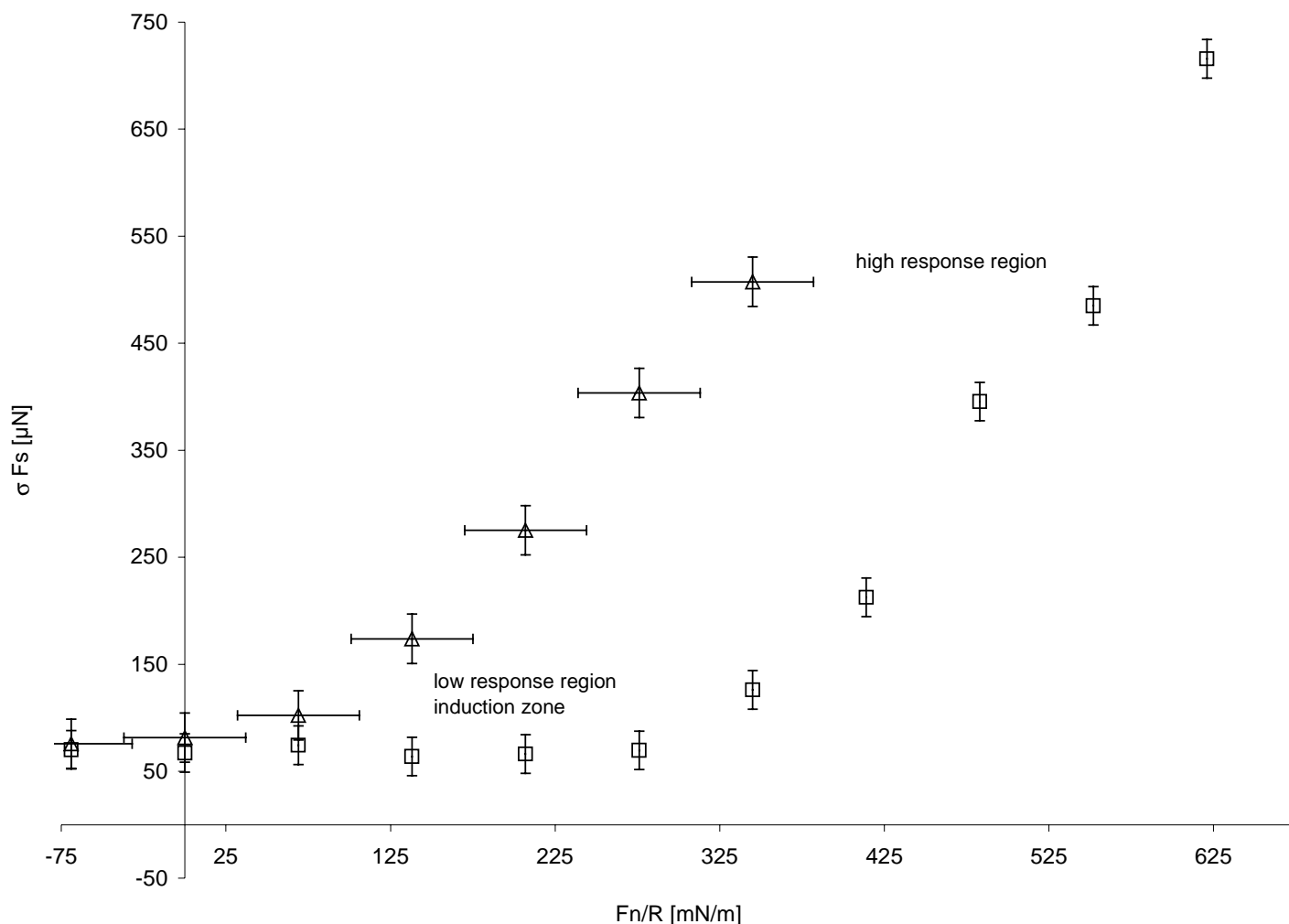


**Figure 3-8:** Graph of two typical measurements (LDPE sheared against CTAB-coated mica in air and ethanol). The first measurement in air (open triangles) shows an immediate response in the air gap capacitor while moving the micrometer carriage expressed in the increase of the values for the standard deviation. The error in x-direction is the standard error of the optical measurement of the vertical movement and valid for all the curves. The y-error is the standard error of the calibration measurement before each compression. In the second measurement in ethanol (open squares) there is first a low response region where no or only a response within the noise level is recorded. At a higher normal load of the two opposing surfaces, there is an increase in response monitored in a higher value of the standard deviation of the shear response. The  $F_s$  value at the negative normal load reflects the uncertainty in the calibration measurement with large surface separations

The more extensive the low response region, the lower the resulting friction between the two surfaces. Basically, an extensive low  $F_{s, \text{response}}$  region implies that greater normal load must be applied in order that, on sliding, a significant shear or frictional force is observed. The high response region is reached at values of  $\sigma$  of  $F_{s, \text{response}}$  that are typically 5 – 10 times higher than the low response region and have a response almost like rigid coupling between the surfaces as can be seen e.g. in Figure 3-7.

The further quantification of the frictional behaviour is as follows: in all cases, the shear response may be viewed as either rising immediately from the lowest loads, in which case a regular friction coefficient  $\mu$  may be estimated from the slope of the friction against load plot. Or, for the case of a large induction zone (I), a minimum value of the effective friction coefficient  $\mu_{eff(\min)}$  may be estimated from the point where the friction begins to rise significantly,

$$\mu_{eff(\min)} = \frac{\delta F_s}{L_0} \quad (3.4)$$

where  $\delta F_s$  is the shear force uncertainty in the induction zone, and  $L_0$  is the load at the end of the induction zone.

Figure 3-9 gives a schematic view for the terms for the determination of  $\mu_{eff(\min)}$

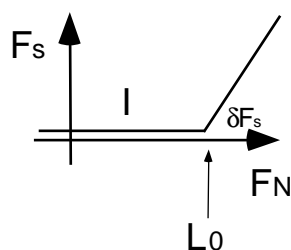


Figure 3-9: schematic of the regions I,  $\delta F_s$  and  $L_0$  to determine  $\mu_{eff(\min)}$

### 3.5 Contact Angle Goniometry

The surface energy of the modified surfaces was determined by contact angle measurements. This approach was used to qualitatively determine whether hydrophilic PEO segments were exposed at the surface of PEP or LDPE blends with PEP-*b*-PEO or PE-*b*-PEO and PE-*g*-PEO block copolymer respectively. The contact angle of water droplets was measured using the contact angle goniometer (Ramé-Hart, equipped with a CCD camera). Pictures from the droplets on the surface were digitised via a frame grabber to a PC and evaluated with the RHI software package. To provide consistently controlled environmental conditions (more than 85 % relative humidity), a chamber with humidity control was constructed.

The surface energy of different substrates can be calculated from measurements of the contact angle of a liquid with known surface tension according to Young's equation (3.5)

$$\gamma_{sl} = \gamma_{sv} - \gamma_{lv} \cos \theta \quad (3.5)$$

where  $\gamma_{sv}$  is the tension between the solid and the surrounding vapour and  $\gamma_{lv} \cos \theta$  is the tension formed between the liquid and the vapour described by the angle  $\theta$  between the two medias, i.e. a hydrophobic surface has a high contact angle with

water and the more the surface becomes hydrophilic the lower the contact angle will be.

### 3.6 Small Angle Neutron Scattering

Small Angle Neutron Scattering (SANS) was used to investigate structural changes in bulk polymer blends. SANS is an indirect scattering technique based on the fact that the wave vectors of elastically scattered neutrons detect different scattering centres depending on different scattering lengths  $b$  of each nucleus. The SANS method is measuring in the reciprocal space and one gets structural information by averaging statistically over the bulk volumes.

In *Figure 3-10*, one can see the wave path of the neutron scattered within two spheres of different sizes where the neutron is described as a wave with wavelength  $\lambda$  and wave vector  $\vec{k}$  before being scattered

$$\lambda = \frac{2\pi}{|\vec{k}|} \quad (3.6)$$

and

$$\sin \theta = \frac{|\vec{Q}|}{2|\vec{k}|} \quad (3.7)$$

where  $|\vec{Q}| \equiv |\vec{k} - \vec{k}'|$  and  $\vec{k}'$  is the neutron wave vector after scattering

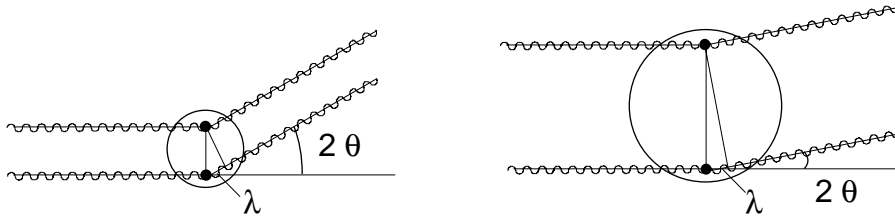


**Figure 3-10:** Schematic drawing of the neutrons wave paths of the scattering centres in two spheres of different size [46] resulting in a change of the scattering angle  $2\theta$ .

The scattering results in the bigger sphere in smaller angles and therefore in smaller scattering vectors  $\vec{Q}$ .

$$\frac{d\Sigma}{d\Omega}(\vec{Q}) = \frac{1}{V} \left| \sum_{i=1}^N b_i e^{i\vec{Q} \cdot \vec{r}_i} \right|^2 \quad (3.8)$$

where  $d\Sigma/d\Omega$  is the differential cross section,  $V$  is the sample volume,  $b_i$  is the coherent scattering length of the atom  $i$  at the position  $\vec{r}_i$  summed over the amount of atoms  $N$ .

The defining property of a crystalline structure is that it is periodic in space. The condition for the constructive interference of scattered neutrons in an angle  $\theta$  is Bragg's law

$$n\lambda = 2d \sin \theta \quad (3.9)$$

where  $n$  is an integer and  $d$  is the distance between two structural lattice planes. Assuming Cartesian coordinates with the origin on a lattice site one can derive this constructive Bragg interference and gets the structural information if the following equation is fulfilled

$$\vec{Q} \cdot \vec{R}_n = 2\pi \times \text{integer} \quad (3.10)$$

where  $\vec{R}_n$  are the lattice vectors of the form

$$\vec{R}_n = n_1 \vec{a}_1 + n_2 \vec{a}_2 + n_3 \vec{a}_3 \quad (3.11)$$

where  $(\vec{a}_1, \vec{a}_2, \vec{a}_3)$  are the basis vectors of the lattice and  $(n_1, n_2, n_3)$  are integers. If one introduces the concept of reciprocal lattice one can find a solution for the equation (3.10). The reciprocal lattice is spanned by the reciprocal lattice basis vectors defined by

$$\vec{a}_1^* = 2\pi \frac{\vec{a}_2 \times \vec{a}_3}{\vec{a}_1 \cdot (\vec{a}_2 \times \vec{a}_3)}, \quad \vec{a}_2^* = 2\pi \frac{\vec{a}_3 \times \vec{a}_1}{\vec{a}_1 \cdot (\vec{a}_2 \times \vec{a}_3)}, \quad \vec{a}_3^* = 2\pi \frac{\vec{a}_1 \times \vec{a}_2}{\vec{a}_1 \cdot (\vec{a}_2 \times \vec{a}_3)}$$

so that any lattice site in the reciprocal lattice is given by

$$\vec{G}_{hkl} = h\vec{a}_1^* + k\vec{a}_2^* + l\vec{a}_3^*$$

where  $\vec{G}$  is the lattice vector and  $h, k, l$  are the Miller indices (integers).

The product of the lattice vector in the reciprocal ( $\vec{G}$ ) and the direct ( $\vec{R}$ ) space is

$$\vec{G} \cdot \vec{R}_n = 2\pi(hn_1 + kn_2 + ln_3) = 2\pi \times \text{integer}$$

and henceforth the solution for equation (3.10) is

$$\vec{Q} = \vec{G}_{hkl}$$

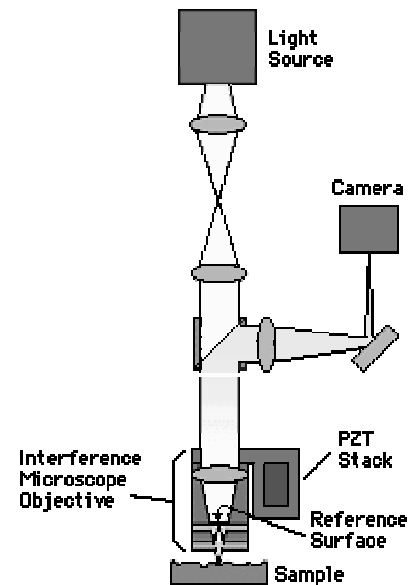
So only if  $\bar{Q}$  coincides with the reciprocal lattice vector a non-vanishing scattering pattern can be seen from a lattice structure.

### 3.7 Optical Phase Interference Microscopy

The non-destructive optical technique (OPIM) is based on scanning white-light interferometry. Incoming light is split inside an interferometer, one beam going to an internal reference surface and the other to the sample surface. After reflection, the beams recombine inside the interferometer, undergoing constructive and destructive interference and producing a light and dark pattern of fringes.

The interference pattern is then pictured by a CCD video-camera and transferred to a frame grabber to digitise the input video signal and process it with MetroPro, a 3-D rendering software provided with the instrument Zygo NewView 200. The vertical resolution is below 1 nanometer and the lateral resolution is below 1 micrometer. The accessible picture size is up to 0.2 x 0.3 mm depending on the optical set-up and offers henceforth a very high vertical resolution with a larger field of view than an atomic force microscope.

Atomic force microscopy (AFM) was used as a supplementary technique to confirm the experimental results received with the OPIM measurements.



## 4 Macro- and Micro-Phase Separation in Polymer Blends

The theories of this section cover the predictions of bulk and thin film properties of pure block copolymer and blends of block copolymer and homopolymer. The intention of the investigation of these systems was to modify the surfaces of the homopolymer with the block copolymer where one end is anchored in the matrix homopolymer and the second block is modifying the surface according to the desired property. Since this block copolymer-homopolymer melts often phase separate, it is appropriate to start with the theoretical background.

### 4.1 Theory

In this section theories dealing with micro-phase separation of block copolymer and macro-phase separation of block copolymers and homopolymers are presented. The first one is related to structures formed in the bulk by block copolymer, which depend on their chain lengths and interaction parameters. The second one describes how an A homopolymer forms an interface with an A-B block copolymer. In the latter, bulk and thin film-conditions are considered.

#### a) Micro-phase separation in block copolymers in bulk conditions

The formation of structures in liquid block copolymer was described by Leibler using a random phase approximation of micro-phase separation [47] and later formulated by Matsen and Bates by a self-consistent field theory [48]. The models suggest that under equilibrium conditions, block copolymers self-assemble in certain configurations, which depend on the product interaction parameter  $\chi N$  (where  $\chi$  is the Flory parameter, characterising the chain interactions and  $N$  the polymerisation index of the blocks) and on the ratio of the block lengths  $f$ . These theories were confirmed by several experiments using SANS and small angle neutron scattering (SAXS) and are described in detail in the literature [49-51]. The phase diagram derived from this theory is plotted in *Figure 4-1*. It shows the phase diagram according to the interaction parameter vs. the block ratios. The phases distinguished are the disordered phase (DIS) for very weak interaction or very high temperatures, the lamellar phase (L) for symmetric block copolymers and the hexagonal cylinders (H), the bicontinuous cubic phase ( $Q_{Ia3d}$ ), the bcc-ordered spheres ( $Q_{Im3m}$ ) and the closed-packed-ordered spheres (CPS) for asymmetric block copolymers depending on the block ratios  $f$  and the Flory interaction parameter  $\chi N$ . In the SANS experiments one can distinguish the phases according to the positions of their Bragg peaks in the Q spectrum.

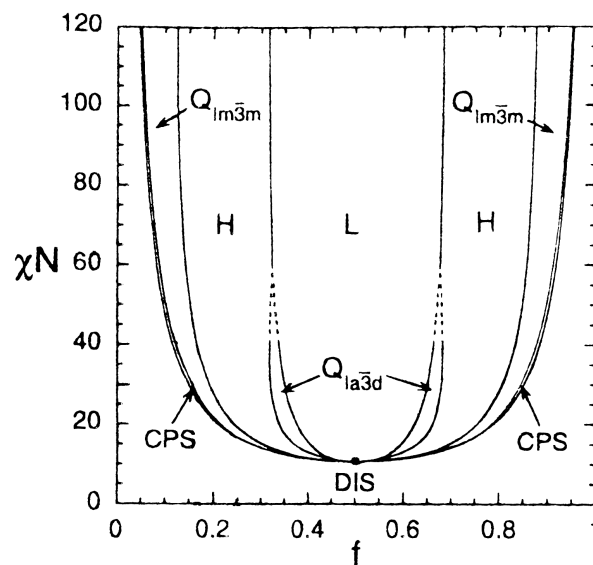


**Figure 4-1:** The phase diagram by Matsen and Bates [48]. Plotted is the interaction parameter vs. the block ratio, showing the different phases. DIS labels the disordered phase where the interaction is small or the temperature is high. The lamellar phase L occurs for symmetric block copolymers. For the asymmetric block ratios, the phases H,  $Q_{1a3d}$ ,  $Q_{1m3m}$  and CPS label the hexagonal cylinders, the bicontinuous cubic phase, the bcc-ordered spheres and the closed-packed-ordered spheres respectively.

b) Macro-phase separation in blends of homopolymer and block copolymers in bulk and thin film conditions

A different issue is that of a block copolymer in a homopolymer matrix. Here the relative chain length of the homopolymer with respect to that of the block copolymer plays an important role.

First discussed is the behaviour of an end-grafted polymer brush put into contact with a homopolymer melt of the similar chemical composition. This system was first described by Leibler *et al.* [52-55] and by Shull [56].

In the model a polymer chain B of chain length  $N_B$  is irreversibly grafted into a continuous layer, forming a dense “brush”. A polymer melt A of similar chemical composition is laid on top. The theory suggests that for a given chain length of the brush forming polymer,  $N_B$ , the final configuration of the system would depend on the chain length  $N_A$  of the top polymer. Two possible scenarios are outlined: the free chains may penetrate into the layer, swell the brush and the excess polymer melt will form a continuous layer on top of the swollen brush. Alternatively, the top homopolymer may minimise the contact with the grafted layer by forming a droplet (this behaviour is the so called ‘autophobicity effect’). The driving force for the penetration of A chains into the grafted layer is the gain of translational entropy while on the other hand the chains in the grafted layer B lose conformational entropy due to stretching of the grafted layer. Only for ratios  $N_A/N_B \leq 1$  are the chains expected to fully penetrate and completely wet the brush (Figure 4-2 a). Long chains A ( $N_A \gg N_B$ ) only penetrate to a certain depth  $\lambda$  (Figure 4-2 c).  $\lambda$  is a measure of the melt-brush interfacial depth and is related to the melt-brush interfacial tension  $\gamma_{mb}$  as:

$$\gamma_{mb} \propto \frac{kT}{\lambda a} \quad (4.1)$$

where  $kT$  is the thermal energy and  $a$  is a molecular length scale.

The model system described above is applicable to binary blends of block copolymers and a homopolymer as will be described in the following paragraphs.

Consider a blend of block copolymer and a homopolymer, where the homopolymer is of the same chemical composition as one of the blocks ( $\chi = 0$ ). Again, the phase behaviour is primarily governed by the ratio of the chain length of the homopolymer ( $N_A$ ) to the block copolymer ( $N_{Ab}$  block length of the same component). In the strong segregation regime, the micro-phase separated regions of the block copolymer may be considered as soft polymeric “brush”-coated “particles”.

If  $N_A \ll N_{Ab}$  (*Figure 4-2 a*), the homopolymer A gains translational entropy, while swelling the A block of the block copolymer. The swelling and henceforth the increase of the interfacial area per A block can lead to changes in the morphology. Furthermore, the osmotic pressure in the micro-phase-separated agglomerates is higher than in the melt and two colloidal particles or agglomerates would repel each other.

If  $N_A \approx N_{Ab}$  (*Figure 4-2 b*), the gain in translational entropy for homopolymer A is not as pronounced as before, since the swelling of the A block results in a loss of conformational entropy.

If  $N_A \gg N_{Ab}$  (*Figure 4-2 c*), macro-phase separation occurs, leading to formation of domains of micro-phase separated block copolymers in a homopolymer matrix. As in the model presented above, the homopolymer penetrates the micro-phase separated domains to typical depths  $\lambda$ . Domains of micro-phase separated block copolymer have a lower osmotic pressure and therefore attract each other and further increase the size of the agglomerates.

Thin films of homopolymer and block copolymer blends will phase separate below a critical temperature into two phases as mentioned previously, because of their unfavourable interaction energy. With asymmetric boundary conditions, an interface will be formed parallel to the substrate due to preferential surface attraction of one of the components, described by Binder for polymer thin films [57]. Depending on the concentration of the two phases and on the interfacial energies between the substrate and the polymer blend, either a continuous layer of one phase at the interface or a ruptured layer, which is characterised through droplets on one of the interfaces, will be formed. One phase will be the micro-phase separated block copolymers and the other the homopolymer.

A continuous layer of block copolymer tends to minimise the interfacial tension and hence the block with the lower interfacial energy will be the first layer. The block at the homopolymer agglomerate interface will be the one minimising the interfacial tension between the A homopolymer and the A-B block copolymer. The A-B block copolymer will be both penetrated and swollen by the homopolymer ( $N_A \ll N_{Ab}$ , *Figure 4-2 a*) or repels the homopolymer in the case of the longer chained homopolymer ( $N_A \gg N_{Ab}$ , *Figure 4-2 b*).

If the block copolymer does not form a continuous layer because of an insufficient concentration or because of unfavourable interfacial tension, the micro-phase separated block copolymer de-wets from the interface and forms droplets. From these droplets where the outer layer would be the one minimising the interfacial tension between block copolymer and the homopolymer the swelling or autophobic reaction follows the same restriction at the interface as for the solid layer. For homopolymer chains being shorter than the block copolymer chain ( $N_A \ll N_{Ab}$ ) the homopolymer would swell the block copolymer and could change the configuration, and for  $N_A \gg N_{Ab}$  the homopolymer would be repelled and de-wet locally from the droplet; a local autophobic effect would appear and craters are formed, whereas the interface with air or substrate is still covered with the homopolymer.

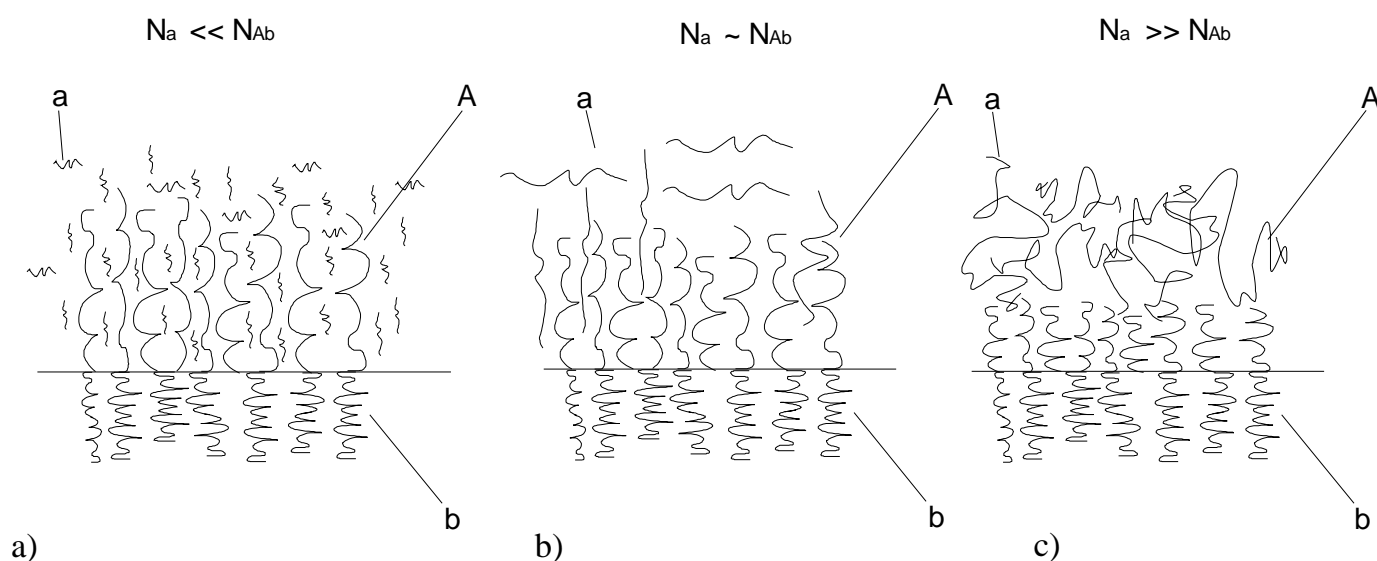


**Figure 4-2:** Schematic graph of the different conditions for the linear block copolymer  $Ab$  in contact with different molecular weights of homopolymer. The block copolymer in the sketch can be either assembled on a hard surface or as a micro-phase separated block copolymer agglomerate. The line between the blocks of the copolymer indicates the sharp interface between energetically non-compatible polymers arising from their high unfavourable interaction energies. In a) the homopolymers  $A$  ( $N_A \ll N_{Ab}$ ) can penetrate the brush  $Ab$ . The osmotic pressure is high and the brush is stretched. In b) the homopolymers  $A$  ( $N_A \approx N_{Ab}$ ) can still penetrate the polymer brush, however the osmotic pressure is lower and the brush is about to collapse. In c) the homopolymers  $A$  ( $N_A \gg N_{Ab}$ ) can not penetrate the brush, the brush collapses and the osmotic pressure is low.

## 4.2 Results

The results of this section cover the investigation of bulk and thin film properties of a block copolymer-homopolymer blend. The intention of the investigation of these systems is to modify the surfaces with the block copolymer where one end is anchored in the matrix homopolymer and the second block is modifying the surface according to the desired property, being for friction reduction a densely tethered polymer brush in a good solvent.

### 4.2.1 SANS: Structural Analysis of Bulk Polymers

All SANS measurements were carried out above the crystallisation temperature of the block copolymers and were done to examine the structure of the pure block copolymer and the block copolymer in contact with the homopolymer.

The SANS spectrum (*Figure 4-3 a*) of the pure homopolymer *d*PEP shows no signals (Bragg-peaks) in the *Q* spectrum. The observed increase for small *Q* values follows Porod's law and indicates large structures [58]. This could be due to the high contrast in SANS of deuterium compared to air and therefore reflects pores in the polymer. In all the measurements, the increasing value in the spectrum at larger *Q* values is due to background noise coming from scattered neutrons from other beam-lines in the measuring hall.

The spectra of the pure linear block copolymer PE-*b*-PEO and PEP-*b*-PEO is very different (*Figure 4-3 b, c and d*). The location of the observed Bragg peak distances is determined by the ratio *f* of the block lengths. In practice for the block ratio *f* one has to take the molecular weight and the density into account. Therefore, *f* is calculated according to the following equation

$$f = \frac{M_{nA}\rho_{nB}}{M_{nA}\rho_{nB} + M_{nB}\rho_{nA}} \quad (4.2)$$

reflecting the theoretical polymerisations  $N_A$  and  $N_B$ , where  $\rho_{nY}$  is the density of block A or B and  $M_{nY}$  is the block molecular weight according to *Table 3-1*. A summary of used block copolymers and their respective *f* is listed in *Table 4-1*.

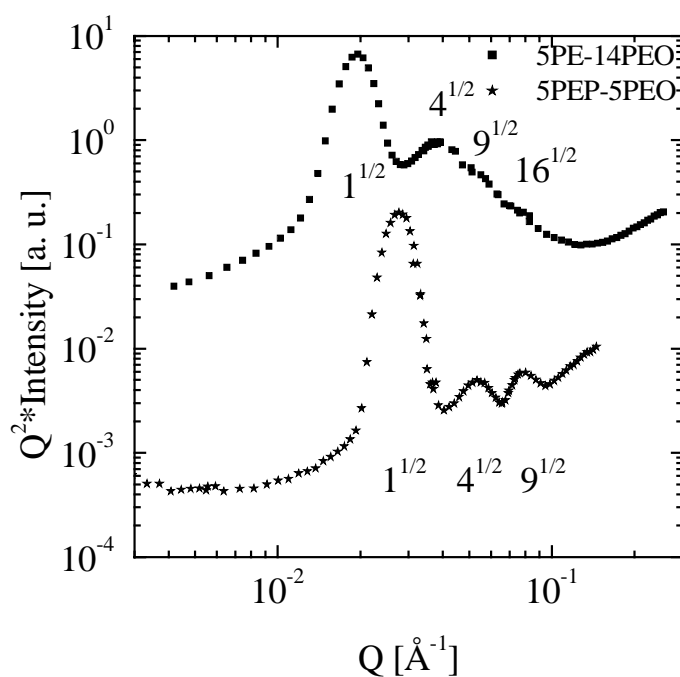
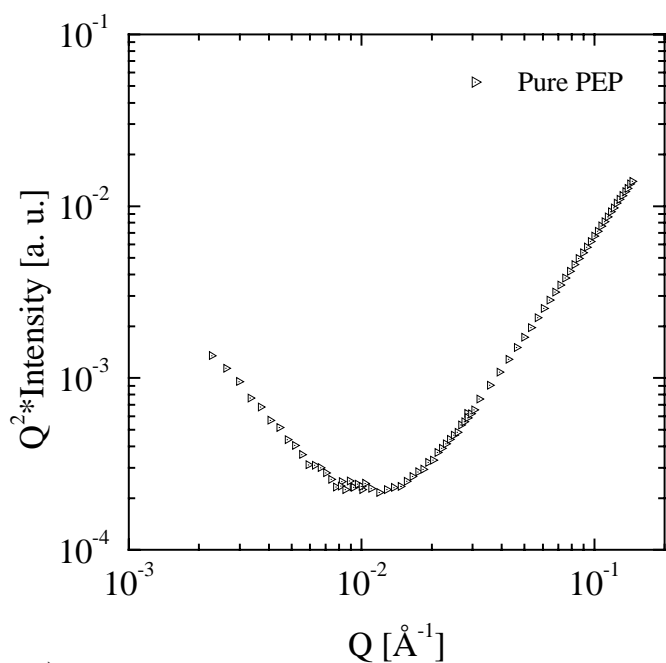
Label of the block copolymer	Block ratio <i>f</i>
<i>d</i> PEP5- <i>b</i> -PEO5	0.5
<i>d</i> PEP5- <i>b</i> -PEO15	0.27
PE5- <i>b</i> - <i>d</i> PEO14	0.35

**Table 4-1:** The block ratios *f* for the investigated linear block copolymers

The symmetric block copolymer PEP-*b*-PEO with *f* = 0.5 and the PE-*b*-PEO with *f* = 0.35 exhibit Bragg-peaks which are separated by factors of natural numbers in between them (*Figure 4-3 b*). This indicates that the block copolymer form a lamellar structure. In the PE-*b*-PEO the second order peak is clearly visible but the third and fourth order peak are only vaguely recognisable. In general, the higher the

order of the Bragg peaks is visible, the more regular is the structure. The damping of higher order peaks is due to the perturbation of the lamellar structure, caused by the proximity in the phase diagram to the boundary to the hexagonal cylinder phase. The position of the first order peak reflects the size of the lamellar spacing in the microstructure. In the case of the symmetric PEP-*b*-PEO second and third order peak are clearly visible, indicating a very regular lamellar structure due to the ideally symmetric *f* for the block ratios in the phase diagram.

The distances between the asymmetric PEP-*b*-PEO block copolymer do not clearly indicate whether a bcc-spheres or hexagonal cylinder structure is preferred. First results (*Figure 4-3 c*) showed a distance profile typical for a bcc-spheres structure, however—relying on the phase diagram—the block ratios should lead to hexagonal cylinders. However, in the first measurement, the pure asymmetric PEP-*b*-PEO block copolymer was not heated above room temperature to fill it in the SANS-measuring quartz cells and therefore the asymmetric block copolymer could have been in a different non-equilibrated state in the phase diagram.



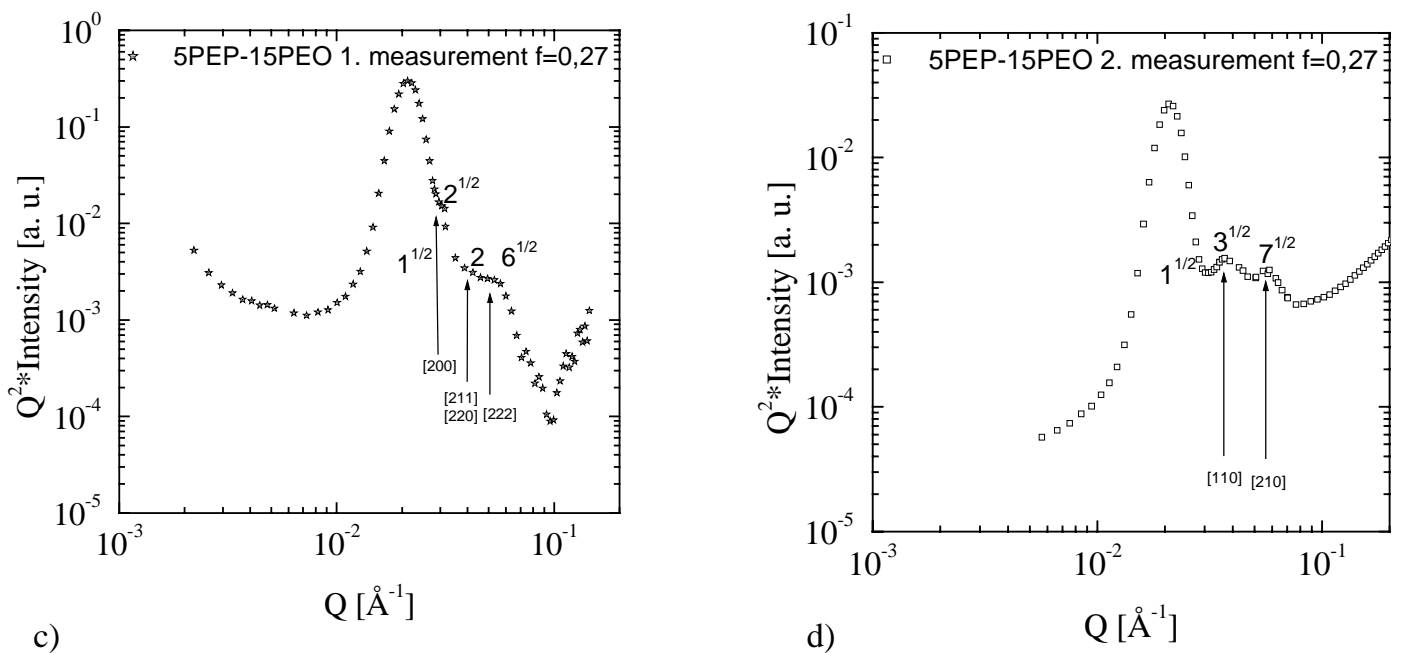


**Figure 4-3:** Different pure polymers measured with SANS showing the micro-phase separated structures. Plotted are  $Q^2$ -corrected SANS data vs. the scattering vector. In a) one can see a graph of homopolymer PEP with a rise for small and big  $Q$  values. The increase in intensity for small  $Q$  values follows Porod's law and indicates large structures [58]. This could be due to the high contrast in SANS of deuterium to air and therefore reflects pores in the polymer. The increase for big  $Q$ -values is due to background noise visible in all the plots more or less intense. In b) a graph of the block copolymers 5PEP-*b*-5PEO (closed stars) and 5PE-*b*-14PEO (closed squares) is plotted; with peaks indicating lamellar structures (curves are shifted for clarity). In c) the first results (open stars) are shown of 5PEP-*b*-15PEO with distances of the Bragg peaks typical for a bcc-spheres structure. In d) the second measurement after heating (open squares) indicates the hexagonal cylinder structure.

In the second measurement the samples were heated up and cooled down as described in chapter 3.2, page 14. The peaks then showed the Bragg peak distances of the hexagonal cylinders. Therefore, it is not clear whether a bcc-spheres or a hexagonal cylinder structure is preferred for the 5PEP-*b*-15PEO-block copolymer. It seems that the bcc-spheres structure was formed, due to a different cooling path where a non-equilibrated structure formed and could not relax to an equilibrium structure during the time of the measurement.

In order to resolve the structural effects of the block copolymer in contact with a homopolymer further measurements were done on blends of PEP homopolymer with incorporated 0.5, 1 and 2 weight percent of block copolymer PEP-*b*-PEO. The Bragg peaks appear at the same positions as the measurements of pure PEP-*b*-PEO. The main difference between the pure and the diluted PEP-*b*-PEO is the scattering intensity, due to a decreased amount of scattering block copolymer in the system. With the reduced scattering intensity also higher order, peaks tend to vanish and are not recognisable any more.

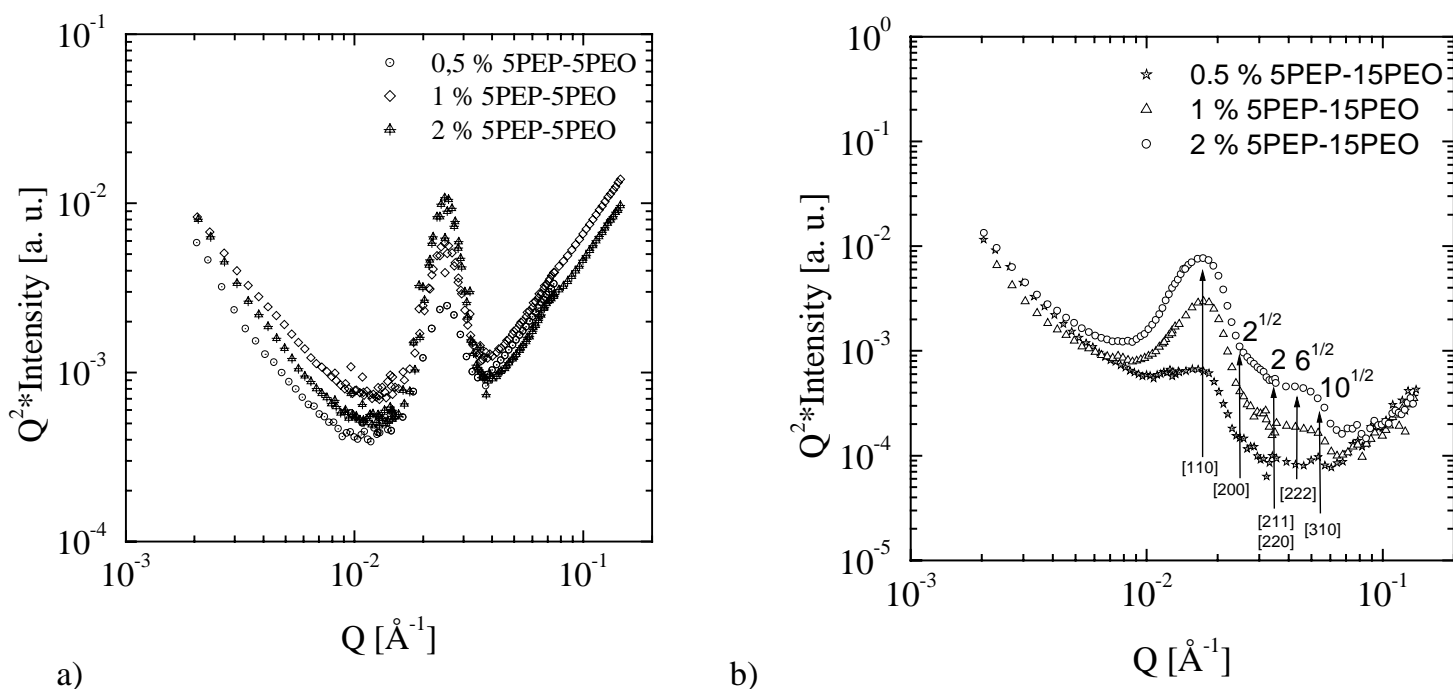


**Figure 4-4:** SANS measurements of block copolymer PEP-*b*-PEO incorporated in a matrix of PEP homopolymer. In both graphs, the influence of the pure homopolymer PEP is visible with the increase for the small  $Q$  values. In a) is the measurement shown of the highly symmetric 5PEP-*b*-5PEO. Visible is only the third order peak for a content of 2 % block copolymer, indicating the lamellar structure in the homopolymer PEP. In b) the asymmetric 5PEP-*b*-15PEO is shown. The arrows mark the broad and not pronounced area of peaks of the bcc-spheres structure. With equal right, one could mark as well the positions for the hexagonal cylinder structure. However, the kink at  $2^{1/2}$  can only appear in a bcc-spheres structure.

This is consistent with the theoretical suggestion that block copolymer form similar structures in the melt and in a matrix of longer homopolymer chains. According to the model, islands of homopolymer and of block copolymer are formed. The structure of the block copolymer within the islands only depends on the ratio  $f$  of the block copolymer tails and is unperturbed by the presence of the long chained homopolymer as predicted by theory.

In the study, only the measurements with pure PE-*b*-PEO were carried out (as there was not the appropriate homopolymer). However, the data with PEP-*b*-PEO, which is a similar block copolymer indicate, clearly the same micro-phase separated structures in blend as in bulk and therefore the similar behaviour for a blend of long chained homopolymer LDPE in contact with PE-*b*-PEO block copolymer is expected.

#### 4.2.2 In Thin Films: Micro-phase Separated Domains Enhancing an Autophobic Effect of the Matrix-Film

With the gained knowledge of the previous SANS bulk measurements of the micro- and macro-phase separated linear block copolymer, now the investigation of

thin films will follow. Therefore, PE-*b*-PEO was incorporated in homopolymer LDPE and the morphological changes were investigated. Surface properties of thin films were mainly investigated using OPIM. AFM was used as a complementary method to investigate the surface morphology and NRA was used for investigation of the depth distribution of deuterated block copolymer in the thin films.

In *Figure 4-5*, one can see a pure LDPE thin film on a Si-wafer as cast (*a*) and after annealing for 120 hours at a temperature of 135 °C (*b*). The following OPIM pictures show areas of 200 x 300 μm.

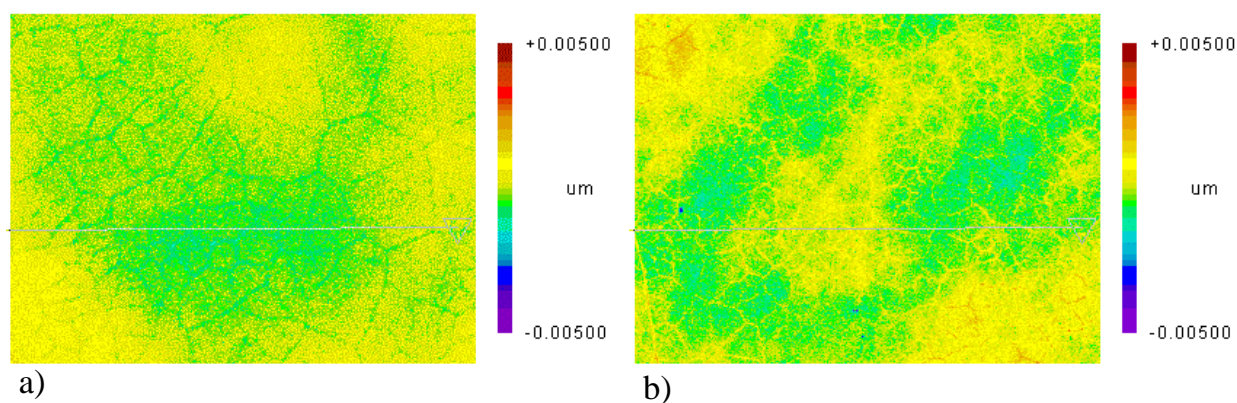


**Figure 4-5:** pure LDPE film as cast (*a*) on Si-wafer and *b*) after 120 hours of annealing at a temperature of 135 °C

It was observed that the presence of block copolymer PE-*b*-PEO in the thin film of LDPE modifies the surface morphology. In *Figure 4-6 a*, one can see the blended LDPE film as cast. In *Figure 4-6 b - d* the blended films were annealed at 135 °C for 12 h, 120 h and 240 h, respectively. It can be observed in *Figure 4-6 a* that small red spots appear with high density, later identified with atomic force microscopy as craters. The size of these red spots was increasing with annealing time and similarly reducing the density of the red spots on the sample.

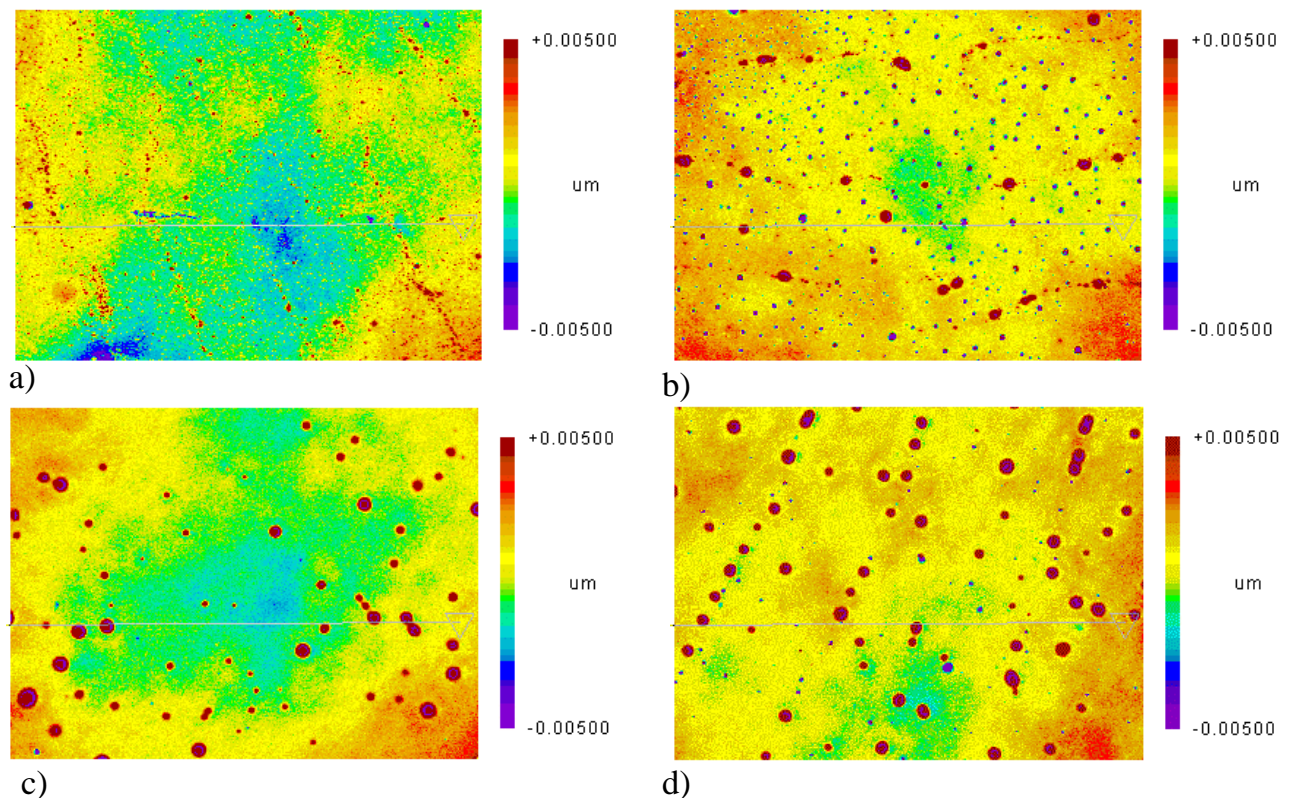


**Figure 4-6:** LDPE films on Si-wafer blended with 10 % of PE-*b*-PEO a) as cast, b) after 12 h of annealing, c) after 120 h of annealing and d) after 240 h of annealing at 135 °C

In *Figure 4-7*, the amount of the red spots (craters) of the pictures in *Figure 4-6 a – d* is evaluated in pixel area.

Area of the red spots is increasing with time of annealing and is an indication for two effects: first the increase of micro-phase separated agglomerates due to the osmotic pressure between the micro-phase separated block copolymers including an attraction to one interface and second the autophobic effect of the homopolymer dewetting from the block copolymer domains. The preferred interface of the block copolymer was investigated with NRA and will be shown subsequently.

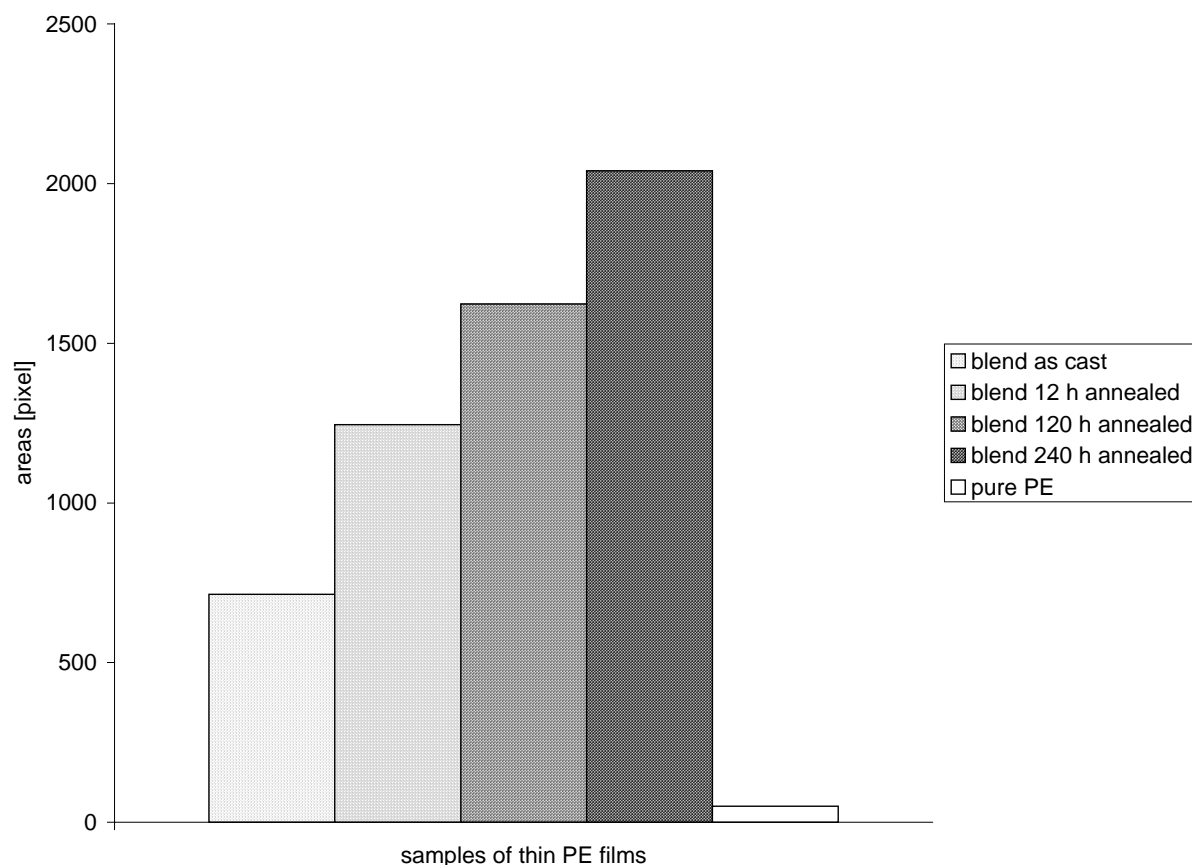


**Figure 4-7:** The size of the red spots in pixel in Figure 4-6 a – d shows an increasing amount of red area with increasing annealing time in the PE-*b*-PEO blended films.

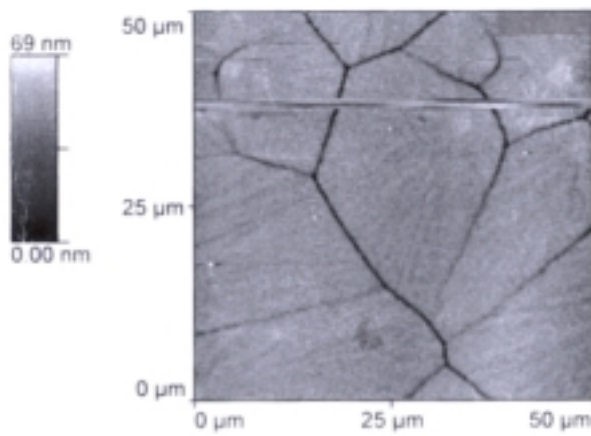
AFM was used for measuring the shape and the topography of the surface as well as the tackiness and the hardness of the surface. In Figure 4-8 a a surface of a pure LDPE is shown and as comparison in Figure 4-8 b and c a surface where PE-*b*-PEO was incorporated. In Figure 4-8 d the height line and the benchmarks labelled with the numbers one to three are shown. The distances and heights between the numbers are presented in Table 4-2 below.

Label	Height	Length
1 – 1	154.5 nm	8.97 $\mu\text{m}$
2 – 2	40.17 nm	6.73 $\mu\text{m}$
3 – 3	6.44 nm	3.51 $\mu\text{m}$

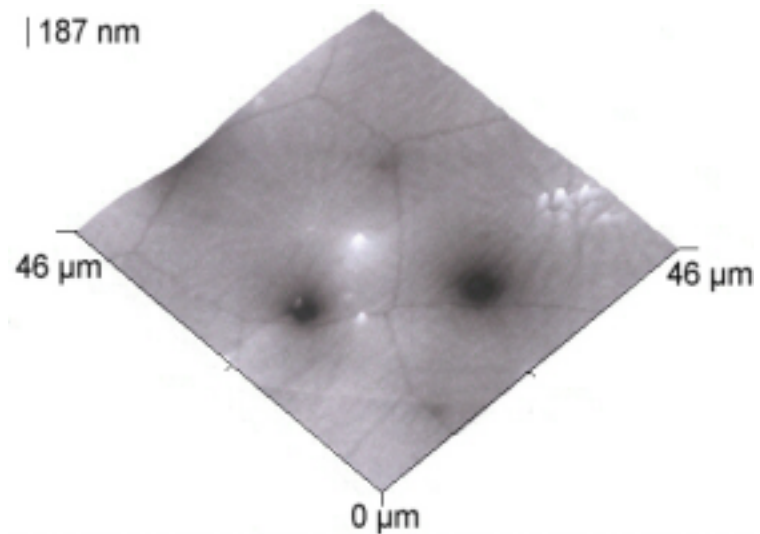
**Table 4-2:** Distances of height and length of the benchmarks of the height line in Figure 4-8 c and d

One can see that the red spots found with OPIM are craters. The measurement of tackiness showed that there is no difference between the top polymer surface outside the hole and the surface in the holes. Both parts showed the same soft

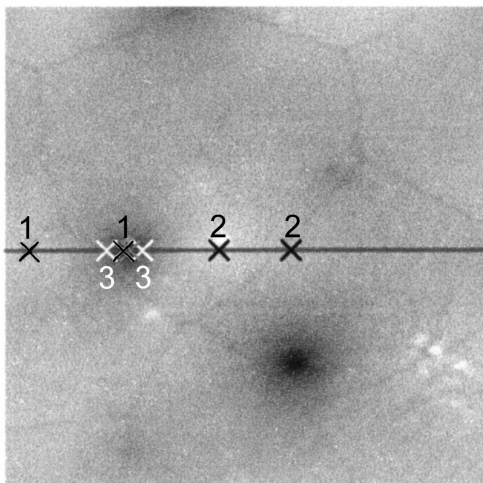
behaviour as one would expect for polymeric surface. This clearly shows that the holes are not reaching the hard silicon wafer.



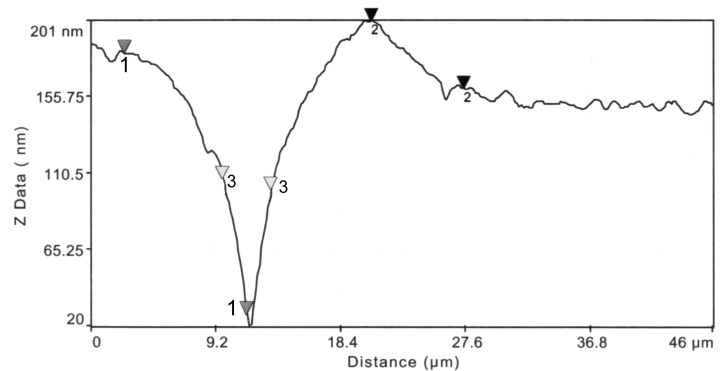
a)



b)



c)



d)

**Figure 4-8:** AFM topography scans of a) pure LDPE film and b) blended film with hole-structure at the surface. The similar picture in c) of the blended film (length 46 μm) with indication of a height line and the benchmarks one to three shown in d).

From contact angle measurements no significant reduction of the water contact angle due to a higher PEO content at the surface could be detected. This suggests that the craters which are forming have no or very little PEO-content at the surface.

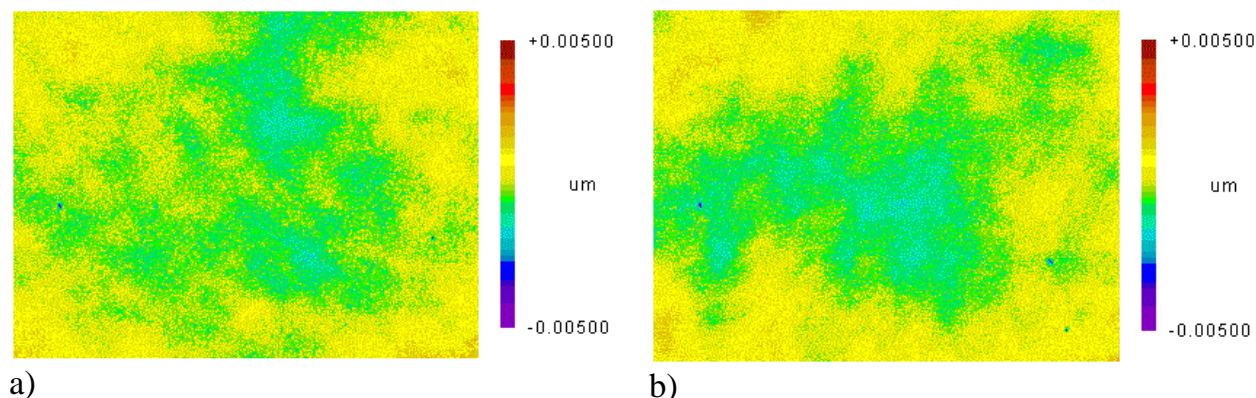


**Figure 4-9:** LDPE films on Si-wafer blended with 5.5 % PE-*g*-PEO2000 a) as cast, b) after 245 h of annealing at 135 °C

Thin films containing homopolymer LDPE and 5.5 % of the grafted block copolymer PE-*g*-PEO2000 (Figure 4-9) were investigated with OPIM. They showed featureless surfaces (as in Figure 4-5 a and b) after spin coating (Figure 4-9 a) and 245 h of annealing at 135 °C (Figure 4-9 b), indicating that the PE-*g*-PEO did not form micro-phase separated structures from which the homopolymer de-wetted. Similarly, also on these surfaces, the water contact angle remained unchanged by introduction of the modifier.

#### 4.2.3 NRA: Depth Distribution of Block Copolymer in Thin Films

NRA was used for the investigation of thin polymer films to distinguish at which interface the block copolymer was accumulated. In all the measurements, the block copolymers were deuterated as listed in Table 3-1 and thus the depth profile reflects the distribution of the block copolymer. In Figure 4-10, NRA-measurements of a blended PEP-film transferred on cross-linked PEP can be seen. In Figure 4-10 a, the cross-link time is 360 s. The graph shows the initial homogeneous distribution of the block copolymer as well as the distribution of PEP-*b*-PEO after annealing for 120 h. One can see that the favoured interface for the PEP-*b*-PEO in a PEP homopolymer laid on cross-linked PEP is the air interface. Samples annealed for 120 hours at 100 °C (slower diffusion) or 170 °C (faster diffusion), showed a similar distribution of the block copolymer indicating that the blend system is in equilibrium. Films that were annealed for longer periods did not show changes in the block copolymer distribution. In Figure 4-10 b, the PEP substrate was non-cross-linked. The graph shows the distribution of PEP-*b*-PEO after 10 h and 120 h of annealing at 100 °C. The observation is that the deuterium concentration at the air surface changes with annealing time. In addition, a penetration of the block copolymer into the non cross-linked layer is observed. When the substrate is PEP that had been cross-linked for 360 s (Figure 4-10 a), almost no block copolymer penetrates the substrate, whereas the non-cross-linked substrate (Figure 4-10 b) shows in equilibrium a homogeneous distribution of the block copolymer apart from the surface enrichment. The 10 h annealed sample (open stars) in Figure 4-10 b, shows the depth distribution of the block copolymer at a non-equilibrium time. The arrow at 300 nm indicates the

presumable interface between the non-cross linked substrate layer and the blended layer. The block copolymer seeks to come into a thermal equilibrium, i.e. a homogeneous distribution and henceforth diffuses into the substrate layer.

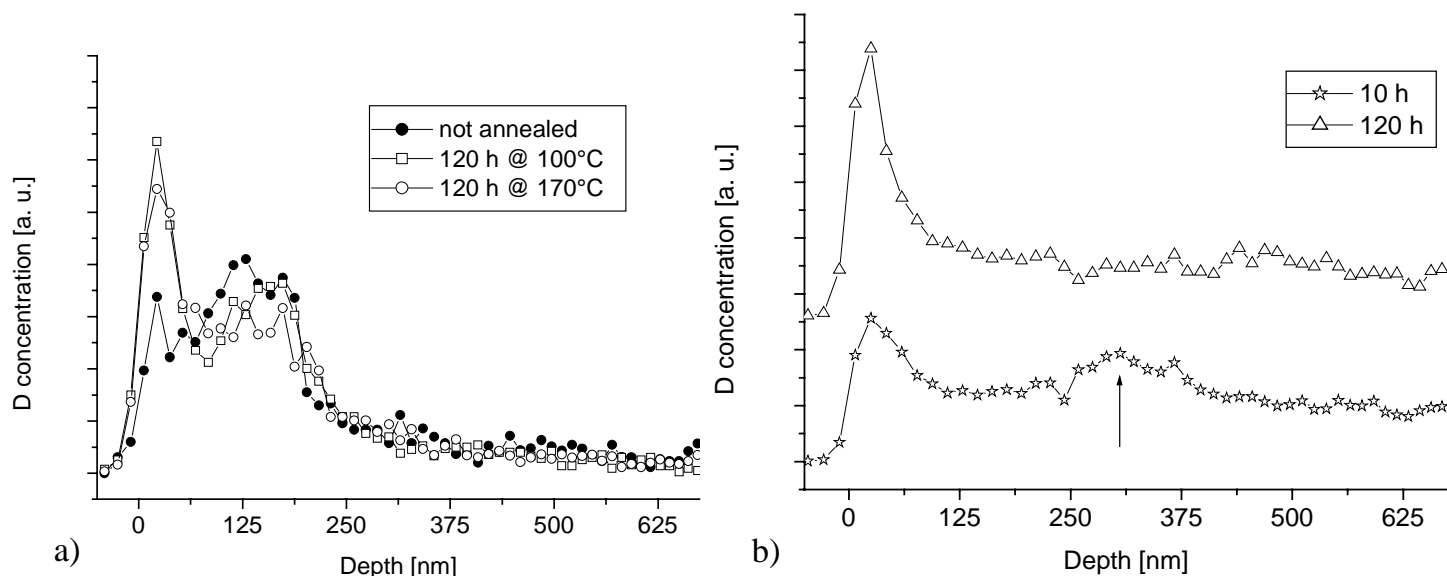


**Figure 4-10:** NRA graphs showing the depth distribution of PEP-*b*-PEO. In both cases, the blended film was transferred on top of a polymeric substrate. One can see the air surface as preferred interface for the block copolymer. The lines serve as guide to the eye. In a) the substrate PEP film is cross-linked for 360 s and therefore impenetrable for the block copolymer. The non-annealed film (closed circles) shows no preferred interface, i.e. the block copolymer is homogeneously distributed in the film. After 120 h, there was no detectable difference between a film annealed at 100 °C (open squares) and a film annealed at 170 °C (open circles). In b) the substrate PEP film is not cross-linked. The non-equilibrium distribution with time can be seen after 10 h (open stars) and the equilibrium distribution after 120 h (open triangles) annealed at 100 °C; the deuterium concentration at the surface after 10 h is not as high, as after 120 h.

In a control experiment, a non-cross-linked LDPE served as a substrate for a film of PEP-block copolymer blend and no penetration of block copolymer PEP-*b*-PEO into the substrate was found. In addition, in this experiment, the block copolymer PEP-*b*-PEO enriched the air surface. Here even the PEP block of the block copolymer is energetically incompatible to the non-cross linked substrate PE-layer and does not penetrate it.

Contact angle measurements were done on these surfaces but no significant decrease of water contact angle was found. The difficulty with floated blend polymer films is that the surfaces are not perfectly smooth after floating. Therefore, it is not obvious whether small variations in the value of the water contact angle are due to different roughness at the surface or due to slightly higher PEO content at the surface.

As a direct comparison to the OPIM and AFM measured films of chapter 4.2.2, NRA measurements were performed on blended thin films directly spin coated on deoxidised Si-wafers and annealed for 120 h at 135 °C. Here blended PEP and LDPE

films show a very similar behaviour. In *Figure 4-11*, one can see that the preferred interface for the block copolymer is the Si-polymer interface.

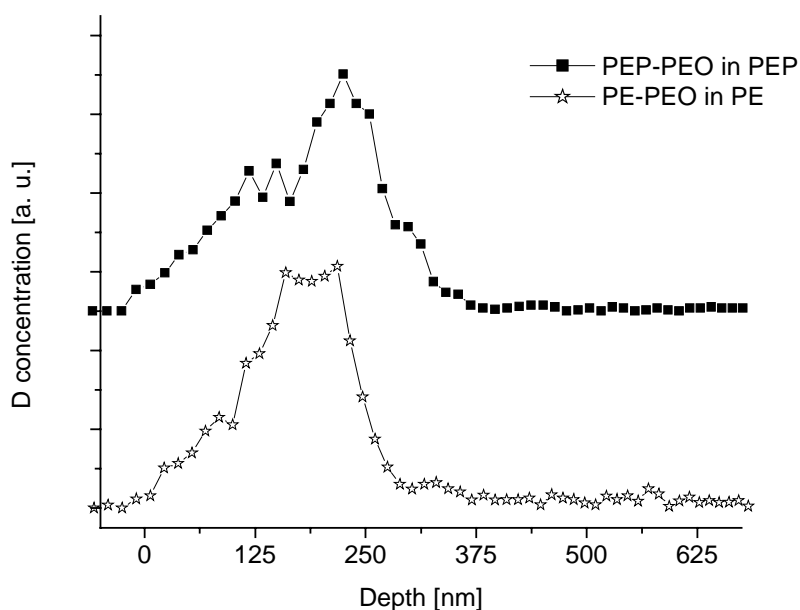


**Figure 4-11:** Graph of an NRA measurement of thin films spin-coated on Si-wafer and annealed for 120 h at 135 °C. The block copolymer enriches the Si-polymer interface, no matter if PE-*b*-PEO is incorporated in a LDPE matrix (open stars) or PEP is blended with PEP-*b*-PEO (closed squares).

The LDPE films used for NRA measurements were prepared in the same way as the samples investigated with OPIM (*Figure 4-6 c*) and AFM (*Figure 4-8 b*). As mentioned above, no reduction in the contact angle compared to the pure LDPE film could be detected. The PEP films were not stable and de-wetted slowly from the Si-wafer when exposed to water. However, contact angle measurements were done on these films, but there was no indication during the measurement for PEO content at the air polymer interface.

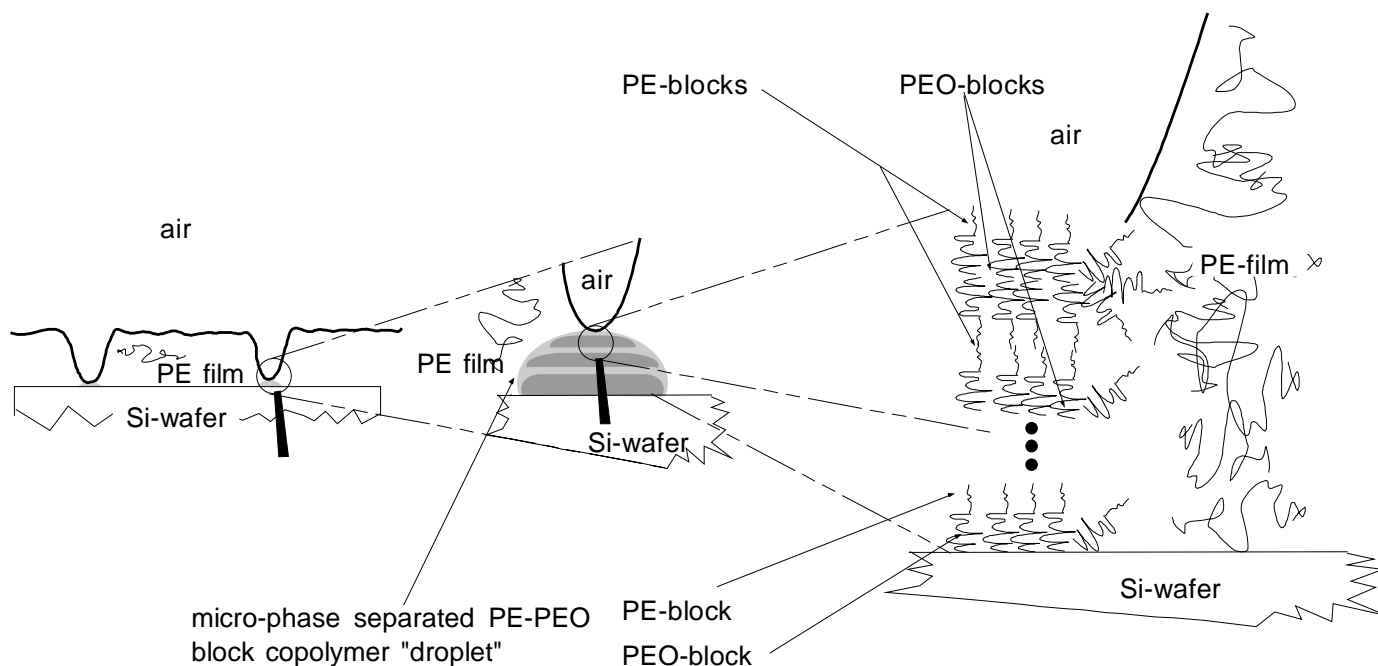


**Figure 4-12:** Picture arising from the results of SANS, OPIM, AFM and NRA for thin films. Idealised graph of the autophobic behaviour of a PE-matrix film from the micro-phase separated PE-*b*-PEO forming a lamellar structure beginning with the PEO block at the Si-wafer

### 4.3 Discussion

The main findings of these sections concern the structure of block copolymers in bulk and thin films. It was found that the structures exhibited in bulk might differ from the ones predicted by the theory and depended on the sample history. It was observed that in thin films the depth distribution of block copolymer depends on film thickness and the substrate surface energy. It was also discovered that in thin films, which contain a blend of a homopolymer and a linear block copolymer, the block copolymers enhance the formation of a crater-like surface structure, due to agglomerates of block copolymer from which the similar long chained homopolymers are dewetting.

In the bulk, at the strong segregation limit, similar structures were observed in films of pure block copolymer and blends, down to concentrations of 0.5 weight percent. This finding was deduced from the similar distances of the Bragg-peaks for pure block copolymer and for blends of block copolymer with homopolymer. The intensities of the Bragg-peaks in the SANS measurements were reduced due to the reduction in scattering material. These findings are consistent with the theoretical predictions described above in chapter 4.1 and the ones described in the book by Hamley [59] and the references therein.

The micro-phase-separation of the pure block copolymer 5PEP-*b*-15PEO and the following controversial structure of the first results could be the reflection of a non-equilibrium structure, due to the history of the PEP-*b*-PEO. The PEP-*b*-PEO was stored at -20 °C and was not heated up above the melting temperature of the PEO

block during preparation. It is not known what happened to the PEP-*b*-PEO before storing at -20 °C and therefore a different structure could have been frozen which was not released during preparation. The influence of different histories for semi-crystalline and crystalline block copolymers is described in a review article by Hamley [60]. There, different crystalline structures were achieved by different preparation techniques and cooling paths of the samples. The second measurements after the sample was newly prepared showed the theoretically expected hexagonal cylinder pattern.

The depth composition profiles of thin films showed a dependence on the permeability of the substrate. As the homopolymer substrates (PEP) became less permeable for the block copolymers with increasing cross-linking times the deuterated material was only observed above the substrate film. A similar effect resulted from the usage of a semi-crystalline PE-substrate. In this case as well, a lower concentration of deuterated material was observed (by NRA) in the regimes within the cross-linked substrates.

It was also observed that in thin films the composition profile was affected by the substrate surface energy. When the block copolymer-homopolymer blend was directly spin-coated on the Si-wafer (after removal of the native oxide layer) the block copolymer PEP-*b*-PEO accumulated at the wafer-polymer interface. However, when the low energy substrate LDPE was used, the PEP-*b*-PEO enriched the air-homopolymer interface.

It was also found that the distribution of the deuterated species (PEP-*b*-PEO) changed with film thickness. In the films where the non-cross linked pure PEP film was used as substrate and a blended layer of PEP with PEP-*b*-PEO was laid on top and far away from the Si-wafer, it was found that the preferred interface of the block copolymer was the air-homopolymer interface. When the blend film was directly spin-coated onto the Si-wafer the preferred interface for the block copolymer was the Si-wafer and not the air.

It was not possible to use the cross-linked pure homopolymer LDPE film as substrate for the blended LDPE plus PE-*b*-PEO. Although the pure LDPE films are stable on mica the lowest concentration of block copolymer PE-*b*-PEO additives ( $10^{-2}$  weight percent) makes them very unstable and the films de-wet immediately after spin coating. Therefore, it was not possible to float a blend film on top of a pure LDPE substrate. Surface modification of mica with a layer of CTAB could not prevent the blended LDPE films from dewetting.

In the case of blended films directly spin-coated on deoxidised Si-wafer, it was observed that the surface structure was completely modified. Enrichment of the Si-wafer with linear block copolymers has led to the formation of micro-phase separated block copolymer agglomerates from which the homopolymer de-wetted. Dewetting was previously deduced from a combination of techniques: Light microscopy and NRA. The extremely low counting rates measured in the NRA experiments (~ 10 cts/h) suggested that a homogenous layer did not form at the interface.

This non-homogeneous layer could be seen by introduction of a linear block copolymer in the thin homopolymer film. The surface changed from a flat surface, where only the crystallisation structures of the pure LDPE could be seen, to a crater structure developing with time. The creation of the crater structure was monitored

with OPIM and AFM. These craters indicated the positions where the micro-phase separated block copolymer agglomerates formed and grew at the Si-wafer. Since the homopolymer matrix material is much longer ( $M_w = 148$  kg/mol) than the similar block of the block copolymer ( $M_w = 5$  kg/mol) the autophobic behaviour of the homopolymer with dewetting from the block copolymer is very likely. The water contact angle is usually an indication for slight surface energy changes, but this sensitive tool showed no significant change expected by placing a droplet on a pure LDPE surface compared to a blended film with crater structure after annealing of several days. This indicates that at the air surface, it is not PEO-tails that are sticking out of the surface, but rather the top layer is formed by PE. In addition, a dewetting of the whole film from the Si-wafer is unlikely, since even with longer annealing periods, a typical dewetting pattern (break-ups of a fingering pattern) was not created. In addition, the AFM tackiness measurements as well as the surface energy measurements with the water contact angles were performed. Both measurements gave no indication for a non-polymeric hard surface or a surface with changing surface energy.

Thin LDPE films blended with PEP-*g*-PEO instead of PEP-*b*-PEO did not form a crater structure, indicating that the micro-phase separated PEP-*g*-PEO forms a homogeneous layer across the film.

A slight increase of block copolymer PE-*b*-PEO at the air-polymer interface was achieved by spin-coating the blended thin films directly on the deoxidised Si-wafer and then on top of that creating a second layer cast from toluene of homopolymer PEO. However, the high interaction parameter  $\chi = 361 \text{ T}^{-1} - 0.589$  [61] between the LDPE and the PEO led to a very fast dewetting of the PEO layer from the LDPE film only a little area stayed covered by the resulting PEO droplets. After the PEO homopolymer was washed away, the films were investigated by NRA and a homogeneous depth distribution of PE-*b*-PEO was found. Compared to the former measurements this increase can be related to the former PEO droplet area, where the PE-*b*-PEO acts in this case as a surfactant at the interface between the two homopolymers LDPE and PEO.

The general conclusion that can be drawn from this chapter is that the PEO block of neither the linear nor the grafted block copolymers is exposed to the air surface of the LDPE or PEP matrix films. Thus, the PEO could not act as a lubricating enhancing modifier. The LDPE and PEP films have lower surface energies than the PEO and therefore it is unfavourable for the PEO to modify the surface. For the linear block copolymer a formation of micro-phase separated agglomerates is observed which was not observed in the case of introduction of grafted block copolymers. In the following chapter it is described how the grafted block copolymer, by preparing solvent cast films on glass, can be made to expose the PEO block at the glass surface and thus to provide precisely that lubricating layer we are looking for.

## 5 Frictional Properties of Modified LDPE-Surfaces

Prior to describing the measurement of the lubricating properties of surface-attached polymer later in this chapter, some theoretical ideas are presented on polymer brushes under various conditions such as good solvent,  $\theta$ -solvent and bad solvent conditions.

### 5.1 Model Calculations for Brushes in Different Solvent Conditions

End-attached polymer chains were described earlier in chapter 4.1 with respect to the swelling and wetting behaviour of a melt laid on top of the “brush”. Now, the properties of this brush in respect to its behaviour under variable solvent conditions will be considered.

The properties most interesting for theoretical investigations were the density and the thickness of the so-called brushes depending on the degree of polymerisation. A common theoretical and experimental picture for polymer chains under good solvent conditions is that the chains are stretched out in direction normal to the surface they are grafted onto, with a thickness proportional to the chain length [62-64].

Now, when two surfaces with end-attached chains under good solvent conditions are brought into contact, they repel each other strongly, which is a result of the high osmotic pressure between the polymer segments in the regions where the chains overlap and a result of their compression.

Less attention was given to the case of changing solvent conditions, where not as much is known on stretching of and lubrication by the polymer brushes, or collapsed brushes, depending on the solvent quality [65]. A review is presented by Grest [66] on polymer brushes under different solvent conditions where he also considers frictional modification.

These investigations usually consider good solvent conditions. While there are very many such studies [66] we consider a particular Monte-Carlo simulation by Lai and Binder in more detail, as it illustrates the different behaviour of brushes being sheared in both good solvent and poor or  $\theta$ -solvent-conditions [67-69].

For the Monte Carlo simulations monodisperse polymer chains of  $N = 40$  monomers were grafted with one end to the impenetrable surface ( $xy$  plane). The grafting sites were subject to self-avoidance, fixed on the surface and chosen randomly. Grafting density for the shown simulations was  $\sigma = 0.1$

Temperature was used as parameter to describe the changes in solvent quality. The picture arising with these Monte Carlo simulations (*Figure 5-1*) is the following: At high temperature ( $1/T = 0.3$ , *Figure 5-1 a*), simulating the case for good solvent quality, the polymer is stretched out and the single monomers of the chain try to avoid each other. At low temperature ( $1/T = 0.7$ , *Figure 5-1 b*), reflecting bad solvent

conditions, the monomers are close-packed and form a more collapsed brush structure. The crystalline structure recognised in the picture is due to the fact that for the simulation the monomers were placed initially on a lattice.

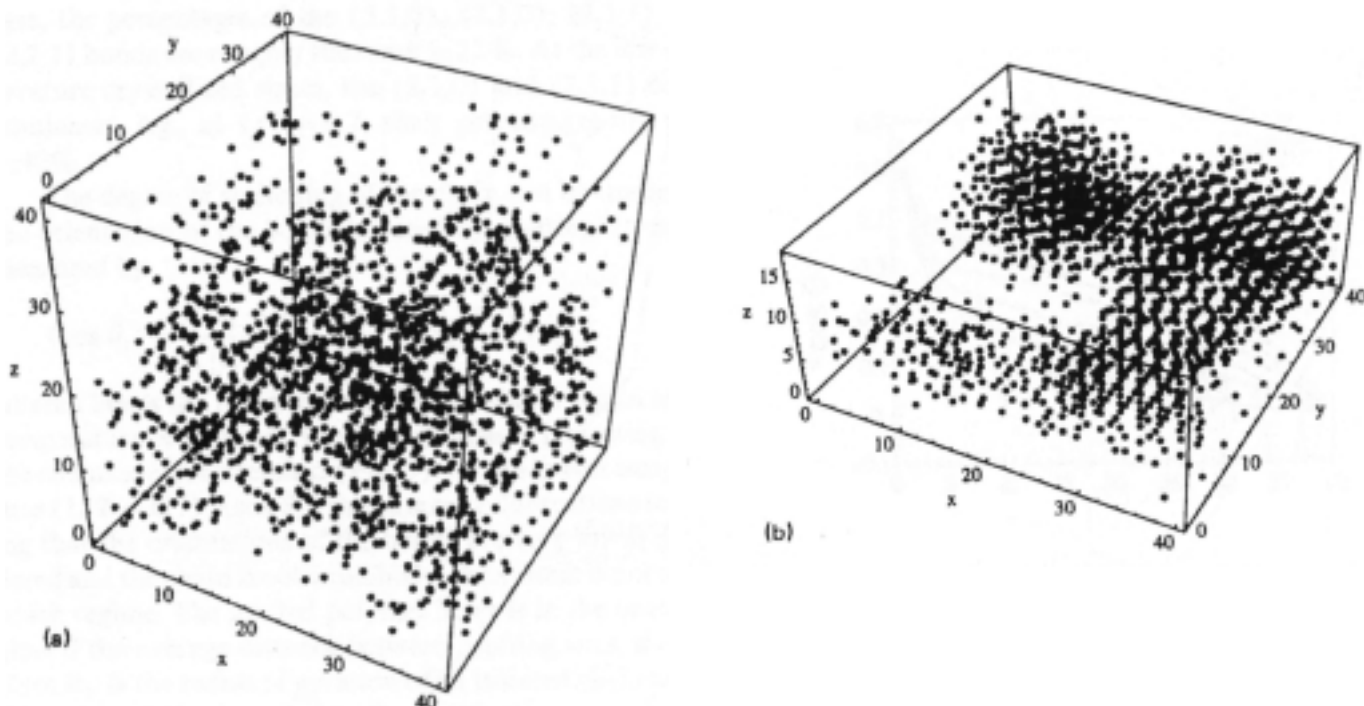


**Figure 5-1:** Monte Carlo simulated monomer distribution for a)  $1/T = 0.3$  (good solvent) and b)  $1/T = 0.7$  (bad solvent) [67,69]

The profiles of the monomer volume fractions  $\phi(z)$  (*Figure 5-2*) become sharper with decreasing temperature. This implies that the polymer brush height decreases and the monomers are confined in a narrower region as the solvent quality of the system decreases.

Another feature visible in *Figure 5-2* is that at the temperatures  $1/T \geq 0.6$  the  $\phi(z)$  decreases rapidly to zero at the brush end. This reflects the discontinuity of the brush end to the solvent because of the phase separation between the monomers and the solvent at which they form a “sharp” interface.

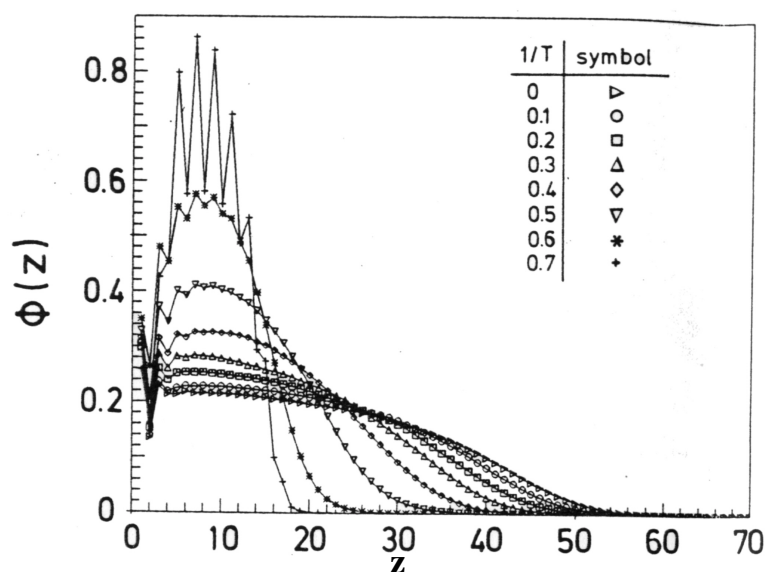


Figure 5-2: The monomer volume fraction  $\phi(z)$  at various temperatures.

The smoothing out at the chain end is due to the finite chain length in the Monte Carlo simulation. The oscillations visible for  $1/T = 0.7$  are due to the close packing and the layering of the simulated monomers.

The same authors also performed Monte Carlo simulations on shear of polymer brushes [70] with changing shear rates but not with changing solvent conditions. They found, as expected, with increasing shear rate a decreasing of the brush height going in hand with a reduction of the “flexibility” of the chains. They claim that this reduction in flexibility is due to the stretching of the chains during the applied shear.

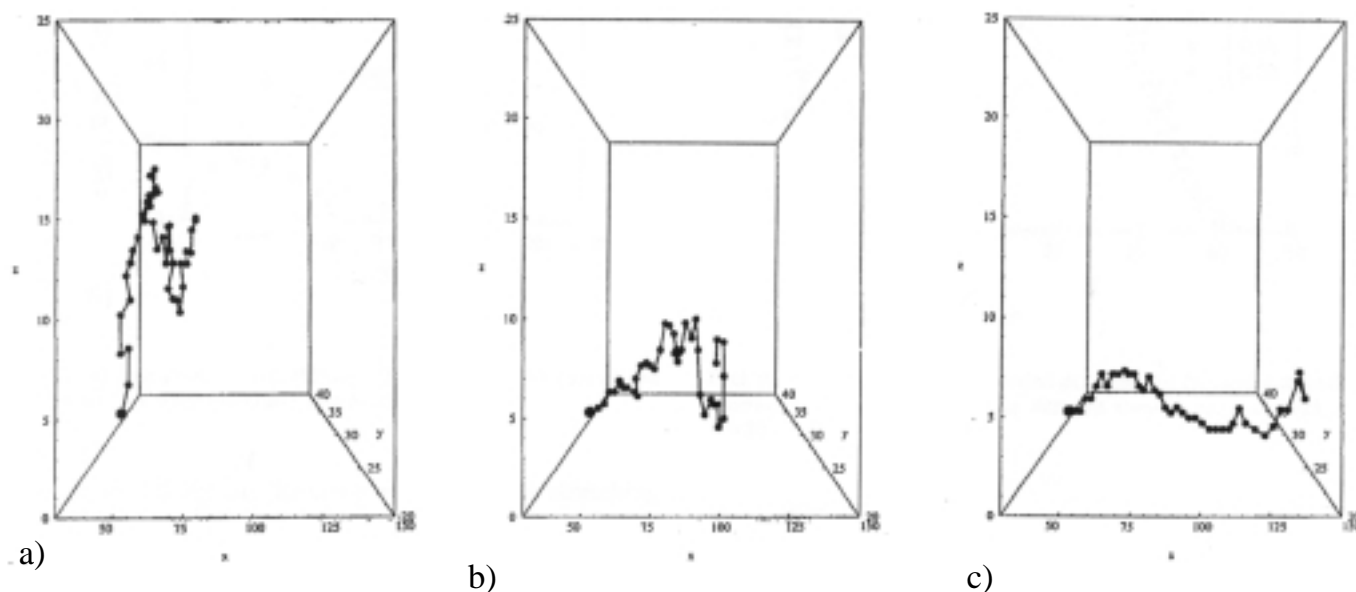


Figure 5-3: Snapshots of brush chains simulated under different shear rates [70]. One chain is represented out of 40. a) lowest shear rate  $\dot{\gamma} = 0.09$ , b)  $\dot{\gamma} = 0.9$  and c)  $\dot{\gamma} = 9$

One can see this reduction in flexibility corresponding to a situation where the brushes are more solid-like.

Simulations by Grest [66] suggest for low shear rates an almost non-reduced brush height. Only for high shear rates a flattening of the polymer brush is observed.

## 5.2 Results

In order to test the surface modifications with respect to their lubrication enhancing properties, the surfaces were compressed and sheared against each other under various conditions. The following section deals with these shear response results.

Striking changes of the frictional behaviour can be seen by shearing different systems of surfaces immersed in different solvents against each other. Not only do the solid or soft solid materials influence the friction greatly but also the solvent in which the surfaces are immersed. Obviously, no common solvent was found that was equally good for every investigated system but with the following results an understanding of brushes and collapsed brushes as well as of solid like friction behaviour could be achieved.

The solubility of the brushes under various conditions seems to influence the lubricating behaviour; therefore, the solubility of the homopolymers supposedly acting as brushes was tested. The solubility of the PEO homopolymer can be different, depending on the molecular weight for the different solvents used. PEO is soluble in H<sub>2</sub>O for every molecular weight. Using PEO homopolymer (Merck) in ethanol the observation was that PEO having a molecular weight less than  $M_n = 1000$  g/mol—therefore also the homopolymer PEO750 with  $M_n = 750$  g/mol, the grafted block in PE-*g*-PEO750—was soluble whereas the one with molecular weight of  $M_n = 2000$  g/mol (PEO2000) was non soluble at room temperature.

In *chapter 4* it was shown that neither the linear nor the grafted block copolymer modifies the surface in respect to its water contact angles. Here solvent cast films, of graft block copolymer incorporated in an LDPE matrix film, on glass were used, where it emerges that the surfaces in contact with the *glass* substrate do expose the PEO block copolymer. As an indication for the hydrophobic and hydrophilic properties of the surfaces, the contact angles (CA) for H<sub>2</sub>O were measured on pure LDPE, and for the modified LDPE-surfaces. The CA (details in *Table 5-1*) found for the pure LDPE and pure PEO were about 90° and almost 30° respectively, where receding CAs were about 5° – 8° less than the advancing ones depending on different surfaces and positions on the surface. The CA for the pure homopolymer PEO has to be interpreted with care and should be viewed only as a tendency since the CA was varying strongly with the time the H<sub>2</sub>O drop resided on the surface. H<sub>2</sub>O first swelled and then dissolved the polymer and at that point, no CA was measurable anymore. The lowest advancing CA found for the modified LDPE surfaces, whether PE-*g*-PEO2000 or PE-*g*-PEO750 was used, is about 70°. The receding CAs were measured as low as 33°. The error for the given angles is about 2° – 4° and is the variation from several measurements at different positions of the surfaces and from different surfaces.

Material	Advancing CA	Receding CA	$\Delta$ adv/rec CA
Pure LDPE	$88^\circ \pm 3^\circ$	$81^\circ \pm 2^\circ$	$7^\circ$
Pure PEO *	$27^\circ \pm 4^\circ$	$21^\circ \pm 3^\circ$	$6^\circ$
10.5 % PE-g-PEO750 in PE	$67^\circ \pm 4^\circ$	$33^\circ \pm 4^\circ$	$34^\circ$
10.7 % PE-g-PEO2000 in PE	$70^\circ \pm 3^\circ$	$43^\circ \pm 2^\circ$	$27^\circ$

**Table 5-1:** Averages of the advancing and receding CA for pure and modified materials.

\* The CA for the pure PEO shows a tendency and indicates the hydrophilicity.  $H_2O$  first swelled and then dissolved the polymer. The measurement was carried out within a minute after the drop was placed on the PEO surface.

The differences in the advancing and receding CAs for the pure materials were rather low and therefore likely to reflect a value close to equilibrium for the CA and for a homogeneous surface energy. For the modified materials a bigger difference of advancing and receding CA was observed. This suggests that more pinning centres on the surface led to a broader distribution around the equilibrium value of the CA. These pinning centres could be the pure LDPE in the case of the advancing CA, whereas the PEO seemed to form pinning centres for the receding CA measurement. It can also be inferred that there are islands of either high or low energy areas, PEO or LDPE, respectively, i.e. not a homogeneous single surface energy was created by modifying the surfaces, but certain islands of PEO blocks were sticking out of the LDPE surface.

### 5.2.1 Polymer and Modified Polymer Sheared against Mica

One knows from SFB measurements that the simple liquids cyclohexane or toluene under compression between smooth surfaces showed solid-like behaviour and that a yield force was required to slide the smooth mica surfaces when the liquids in the gap between them were compressed to a few monolayers or less ( $\leq 6$ ) [15-17,19,71-73]. In contrast, in measurements of pure conductivity water and water with NaCl (0.001 – 0.1 M) no change in the viscosity and no solid-like shear behaviour was observed to the measurable resolution [74,75], though up to normal stresses of a few atmospheres only.

When polymer chains were end-attached on the mica surface establishing a brush layer, the friction was drastically reduced if the brushes were immersed in a good solvent between the compressed surfaces [20,21,23-25,76,77]. Few measurements with brushes in poor or non-dissolving liquids have been published [78].

In the case where thick crystalline or semi-crystalline polymer films are sheared against a mica surface, we would expect that the brush-modified surfaces would experience reduced friction compared to the non-modified polymer film due to the same “entropic lubrication” mechanism as for interacting polymer brush does in the model system where the polymer chains are end-attached on a mica sheet [21,23-25,63,64,76].

The polymer surfaces are sheared against atomically smooth mica surfaces in order to avoid influences of microscopic roughness from which most other solid surfaces suffer.

The first system measured, and always used as a baseline for comparison, is the pure LDPE surface sliding across a mica surface under various conditions. The shear response is plotted in *Figure 5-4* for different conditions between the surfaces. One can see that no matter whether air, ethanol or conductivity H<sub>2</sub>O was used, no significant changes of the shear response could be observed.

When the LDPE was modified by addition of PE-*g*-PEO750 and PE-*g*-PEO2000 as modifiers to the LDPE matrix, a long induction zone could be observed indicating a good lubrication that was achieved in the presence of H<sub>2</sub>O as can be seen in *Figure 5-4* and *Figure 5-5*. The PE-*g*-PEO750 seems—possibly due to the lower molecular weight PEO side chain and the therefore lower regime of compressibility before the surface modifying layer becomes solid-like—to have a shorter induction zone and therefore implies that it reduces the friction less than the higher molecular weight side-chained PE-*g*-PEO2000-modifier. The extremely low increase of the slope of the shear response curve of the PE-*g*-PEO2000 measurements in H<sub>2</sub>O with high normal loads between the surfaces also indicates the low friction response for the two surfaces sliding past each other.

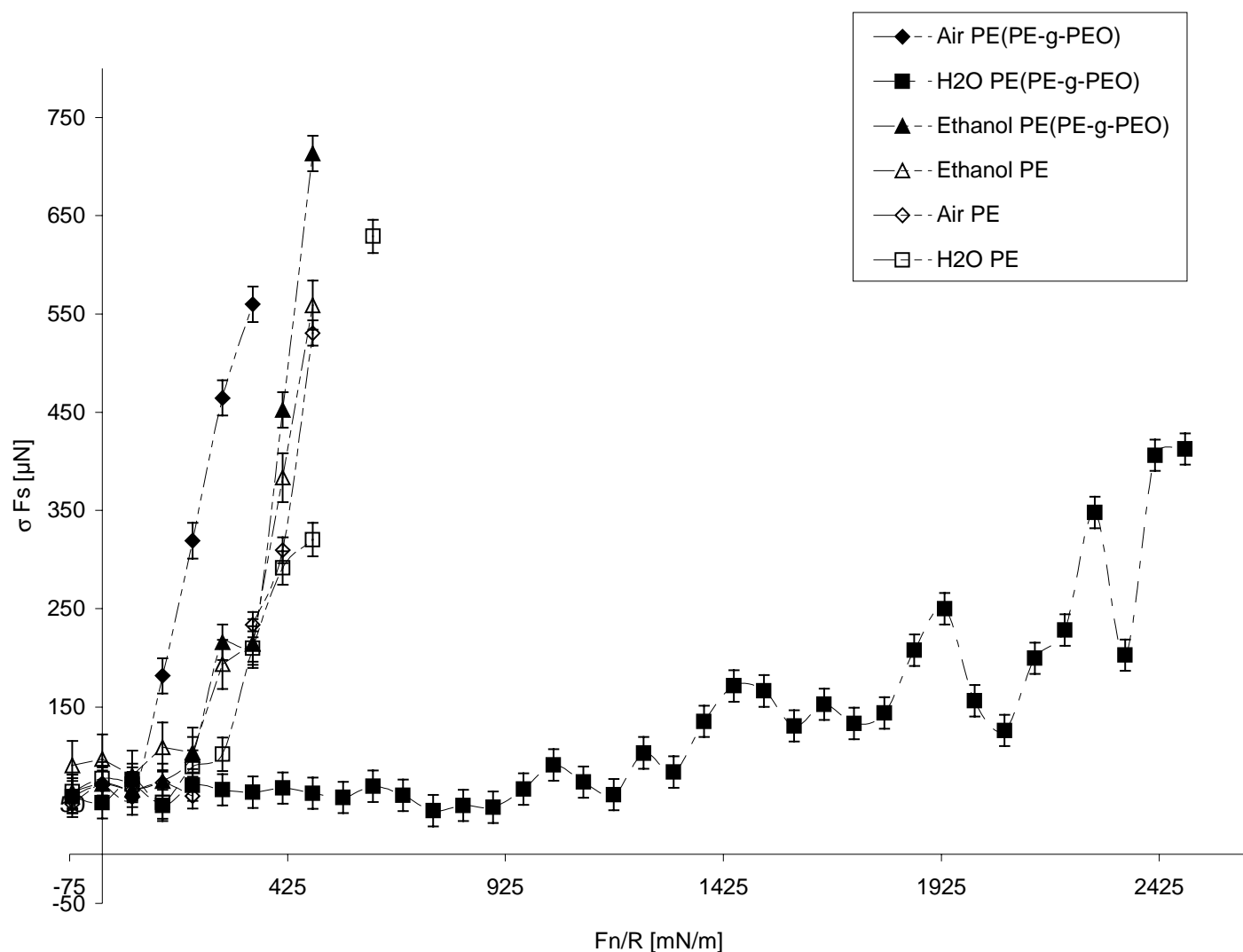


**Figure 5-4:** Comparison of the shear response of the pure LDPE (open symbols) sheared against mica and the 10.7 % PE-*g*-PEO2000-modified LDPE (full symbols) against mica in air, ethanol and conductivity H<sub>2</sub>O. The curves show that the immersion liquid has no effect on the frictional behaviour of LDPE whereas for the LDPE modified with PE-*g*-PEO2000 there is a drastic change in friction depending on the immersion liquid. The curve for the system of H<sub>2</sub>O, mica and modified LDPE (full squares) shows the most extreme case in friction reduction for all the measurements and systems.

The measurements with ethanol as immersion liquid gave somewhat different results, probably due to the different solubility of the PEO moieties on the graft block copolymers. Thus, the PE-*g*-PEO750-modified films, when immersed in ethanol, had as long a low-friction-regime as they had with H<sub>2</sub>O as immersion liquid, whereas the PE-*g*-PEO2000-modified surfaces showed a shear response essentially similar to air, indicating ethanol was a poor solvent for the PEO moieties PE-*g*-PEO2000. The results are in line with the earlier solubility results with PEO2000 and PEO750 homopolymers in ethanol.

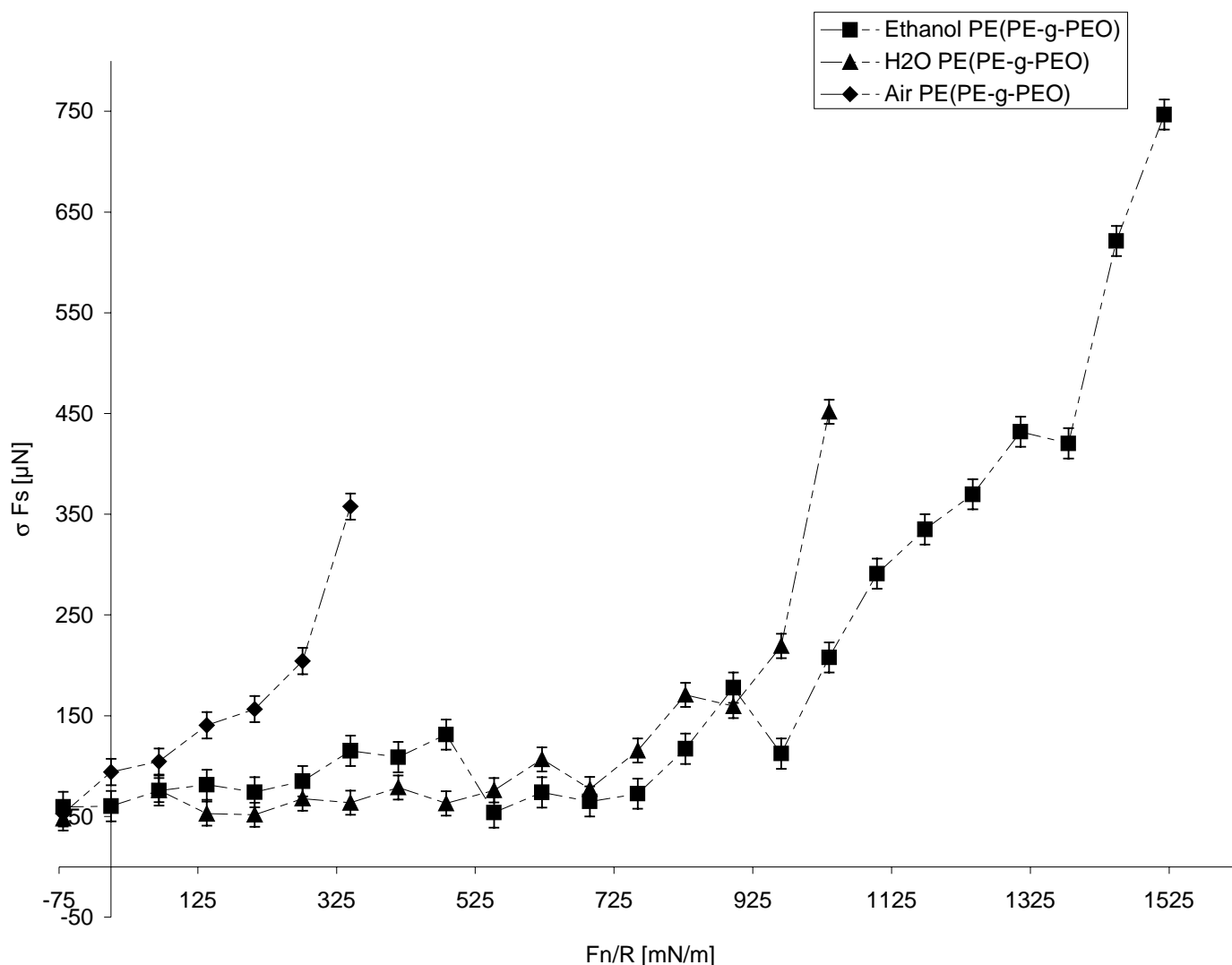


**Figure 5-5:** The curves monitor the shear response of—with 10.5 % PE-g-PEO750—modified LDPE against mica with air, ethanol and conductivity H<sub>2</sub>O. No significant differences can be seen between H<sub>2</sub>O (full triangles) and ethanol (full squares) as immersion liquids.

Measurements with LDPE modified with PE-g-PEO also indicated clearly the dependence on the molecular weight of the modifying substance. The higher the molecular weight of the PEO side chain of the PE-g-PEO, the lower the resulting friction for a given load between the mica and the polymer surface with immersion liquid conductivity water.

Choice of solvent was also important for the enhancing effect of friction reduction in connection with the solubility. The PEO750 was soluble in ethanol and henceforth the LDPE modified with PE-g-PEO750 showed low friction, whereas the PEO2000 was not soluble and the LDPE modified with PE-g-PEO2000 had a high shear response comparable to the friction using unmodified LDPE.

These results gave rise to the idea of a collapsed brush for the measured system of LDPE modified with PE-*g*-PEO2000 and immersion liquid ethanol. The picture of a stretched or solvated brush appears appropriate for the LDPE modified with PE-*g*-PEO2000 or PE-*g*-PEO750 in combination with the immersion liquid conductivity H<sub>2</sub>O. Furthermore, for the case of water as a medium, the higher molecular weight PEO moieties (PE-*g*-PEO2000) provided a better lubrication.

In order to examine the effect of the roughness of the polymer surface on the shear response measurements, solvent-cast films (*Figure 3-4 a*) were used and showed qualitatively the same behaviour as the films that were flattened between two glass slides (*Figure 3-4 b*). The results (not reported in this thesis) indicated that the roughness of the non-smoothed polymer films had an influence on the shear response. The higher roughness of the polymer films reduced the induction zone but also showed that the lubricating enhancing behaviour of the PE-*g*-PEO in a LDPE matrix stayed qualitatively the same as with smoother surfaces.

### 5.2.2 Polymer and Modified Polymer Sheared against CTAB on Mica

In order to change the surface characteristics of the polymer opposing surface from high energy and hydrophilic properties (mica) to low energy and hydrophobic properties, the mica surface was coated with CTAB.

Mica coated with CTAB appeared to be perfectly wetted by ethanol, while propanol formed a small finite CA and isobutanol had a somewhat larger CA. Precise measuring of the CA of those liquids was difficult, because they rapidly evaporated and in addition swelled the underlying substrate. However, the tendencies were clearly visible, with the increase of CA for the longer chained alcohols on CTAB. The advancing CA formed by H<sub>2</sub>O on CTAB was  $82^\circ \pm 3^\circ$  and the receding CA was  $35^\circ \pm 4^\circ$ . This indicates on the one hand the hydrophobicity of the CTAB on mica but indicates on the other hand as well a lot of pinning centres for receding H<sub>2</sub>O on the surface.

In *Figure 5-6*, one can see the influence of different solvents on the frictional behaviour of the CTAB-coated mica system against the PE-*g*-PEO2000-modified LDPE polymer surface. Ethanol worked in this system as the immersion liquid with the best friction reduction effect whereas here H<sub>2</sub>O did not act as a lubrication enhancing immersion liquid. The propanol as a medium between the sliding surfaces was still a better lubricant than H<sub>2</sub>O. However, the propanol has a higher viscosity than ethanol or H<sub>2</sub>O. Friction reduction when using isobutanol is almost non-existent and it seems that directly on compression of the two surfaces, rigid coupling occurs at the sheared interface.

Apparently, in the systems where CTAB is coated onto mica surfaces the CTAB acts as a lubricating brush. It reduces the friction during the shear measurements. However, only if the opposing surface is LDPE modified with a PE-*g*-PEO the lubricating effect is observable. When non-modified LDPE slides across CTAB-coated mica with the immersion liquid ethanol, a small reduction in the friction is observed relative to air or water immersion conditions. Further studies with various immersion fluids with a CTAB-coated mica opposing a mica surface with or without

polymer chains end-attached would seem to be appropriate to check the brush like behaviour of CTAB on mica. One can also test the influence of the various solvent or non-solvent conditions. These experiments should be done with the surface force balance where better resolution and higher sensitivity can be achieved.

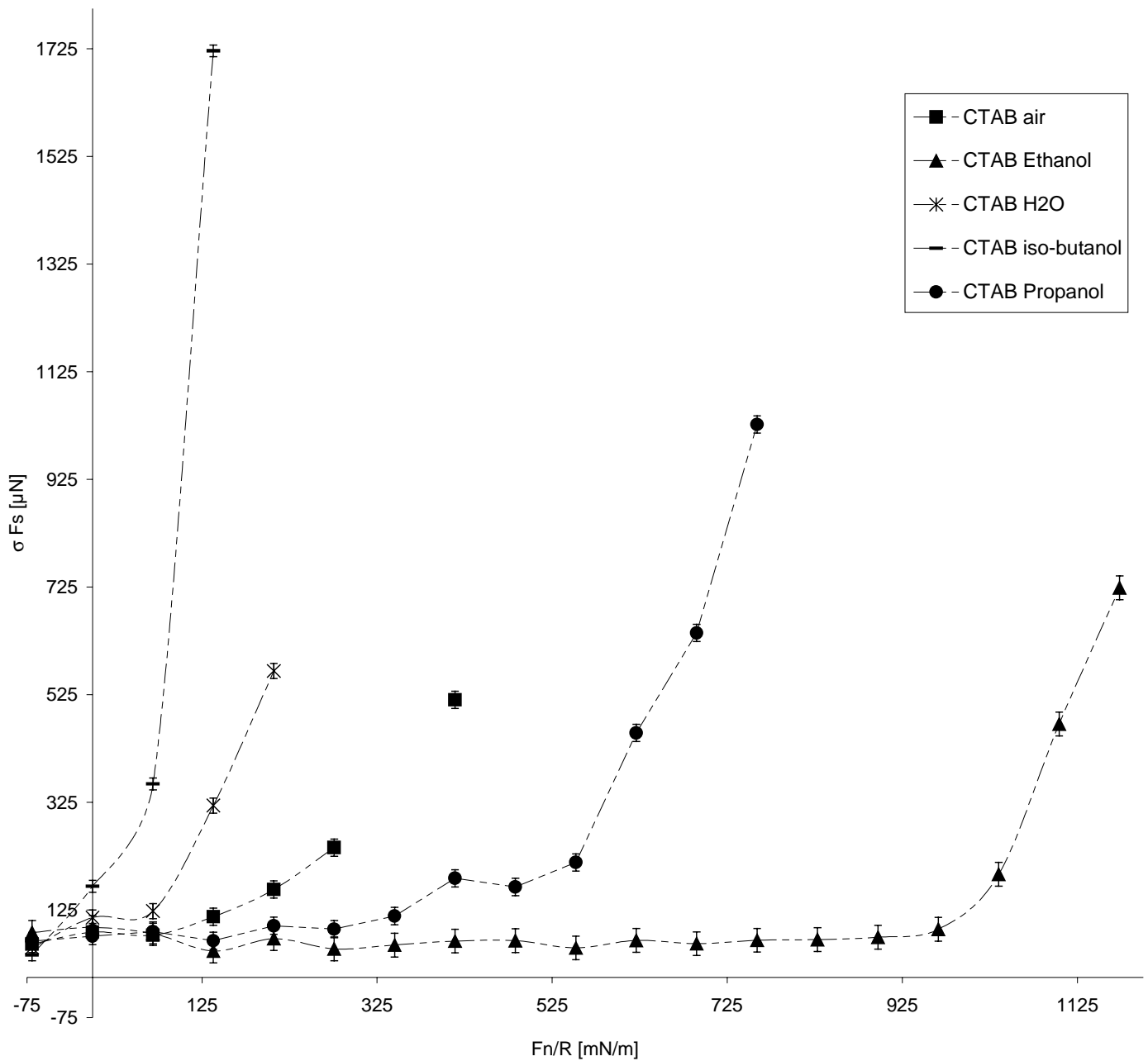


**Figure 5-6:** The graph shows a comparison of the effect of different immersion liquids in a CTAB-coated mica system against the LDPE surface modified with PE-g-PEO2000. Non-modified LDPE does show a slight change in its frictional behaviour but it is not as significant as for the modified case and could be still within the systematic error of one step in the approach.

### 5.2.3 Overview of the Frictional Modification of the Systems Investigated

Although the areas of contact of the surfaces are increasing when a normal load was applied, a shear response was not necessarily immediately present while sliding the surfaces past each other. In the case of low friction, the applied normal load had to be increased in order to achieve the same shear response between the sheared surfaces; this flat region where the load increases with little change in the frictional force is termed the induction zone. The longer the induction zone, the lower the friction. The induction zones are reflecting the frictional properties and provide a useful measure of the friction reduction achieved by different modifications of the surfaces sheared against each other and the immersion liquids used. *Table 5-2* gives a schematic of the frictional behaviour for all the measured systems.

The schematics show the same results as with the above-shown shear measurements. The dependency on the solubility of the top surface layers can be related to the reduction of the friction. One can see that the system LDPE modified with PE-g-PEO2000 sheared versus Mica in water has the longest induction zone. The normal load applied for the same shear response is almost one order of magnitude higher than the same system in the bad solvents air or ethanol. Isobutanol seems to be in a different league with increasing normal load, due to the higher viscosity and different wetting behaviour on the CTAB surfaces than ethanol and propanol. The behaviour of almost rigid coupling during shear is reflected in the immediate shear response.

Solvent	LDPE & "Modifier"	Opposing surface	Schematic of the induction zone (see Figure 3-9)	comments	
Air	LDPE	Mica		Rapid onset of friction at low loads $0.05 \leq \mu_{eff(\min)} \leq 0.08$	
	PE-g-PEO2000				
	PE-g-PEO750				
	LDPE	CTAB			
PE-g-PEO2000					
H <sub>2</sub> O	LDPE	Mica		Longest induction zone—best lubrication $\mu_{eff(\min)} \approx 0.005$	
	PE-g-PEO2000				
	PE-g-PEO750				
	LDPE	CTAB			Large induction zone—good lubrication $\mu_{eff(\min)} \approx 0.007$
	PE-g-PEO2000				
	PE-g-PEO750				
Ethanol	LDPE	Mica			Rapid onset of friction at low loads $0.03 \leq \mu_{eff(\min)} \leq 0.08$
	PE-g-PEO2000				
	PE-g-PEO750	CTAB			
	LDPE				
	PE-g-PEO2000				
	PE-g-PEO750				
Isobutanol	LDPE	CTAB		Apparent adhesion and high friction at low loads. $\mu_{eff(\min)} \approx 0.5$	
	PE-g-PEO2000				

Table 5-2: Graphical comparison of the induction zones indicating a low or high friction regime.

### 5.3 Discussion

The main findings of this section concern the lubrication-enhancing effect of a modifying graft block copolymer acting as a lubricating enhancing layer or a brush-like layer present at the air-matrix interface of polyethylene films. SRA suggests that friction of the LDPE modified surfaces ( $\mu_{eff(\min)} \approx 0.005$ ) was reduced in terms of  $\mu_{eff(\min)}$  by almost one order of magnitude relative to the non-modified LDPE surfaces ( $\mu_{eff(\min)} \approx 0.03$ ). The influences of different immersion liquids and the effect of solubility were characterised.

It was found that the efficiency of graft block copolymers as lubricants depended on the quality of the solvent with respect to the polymer. LDPE surfaces modified with PE-*g*-PEO2000 where PEO2000 is soluble in water reduced the friction when water was used as the immersion liquid. Water as immersion fluid showed an induction region that was longer by a factor of almost 10 compared to air. This indicates a low friction regime even though the areas in contact of the sheared surfaces increased, by increasing the normal load between the surfaces, to a maximum value of  $6.3 \cdot 10^{-9} \text{ m}^2$  (JKR approximation with Young's modulus of  $2 \cdot 10^9 \text{ N/m}$  for LDPE). The corresponding pressure or normal stress is about  $4 \cdot 10^6 \text{ Pa}$  or 40 atm. When ethanol was used as immersion fluid (a non-solvent for PEO2000 at room temperature), the friction with PE-*g*-PEO2000 modified LDPE surfaces was not reduced compared to air, probably because of the collapse of the PEO2000 moieties. The homopolymer PEO750 is soluble in both water and ethanol at room temperature, and consequently LDPE surfaces modified with PE-*g*-PEO750 did have an enlarged induction regime implying that the friction in water and in ethanol equally was reduced by a factor of about five relative to air. These observations are consistent with the Monte Carlo simulations by Lai and Binder [67-69] that suggest that brushes only assemble in good solvents, whereas in  $\theta$ -solvents or poor solvents the polymer chains collapse and form a much denser layer rather than a swollen brush.

The molecular weight of the PEO side block of the modifier block was found to affect the efficiency of the polymers as lubricants: LDPE surfaces modified with PE-*g*-PEO2000 or PE-*g*-PEO750 both enlarged the induction region and imply therefore a reduced friction when immersed in water compared to friction in air. However, the LDPE surfaces modified with PE-*g*-PEO2000 enlarged the induction zone by a factor of 1.5 compared to the LDPE surfaces modified with PE-*g*-PEO750. This implies that the molecular weight and therefore the chain length acting as brush is important to the lubricating effect of the modifier.

It was found that mica coated with CTAB had in some cases a similar effect to that of a polymer brush, i.e. the length of the induction zone indicating the degree of lubrication showed a dependence on the solvent-surface compatibility. LDPE surfaces modified with PE-*g*-PEO2000 sheared against the CTAB coated mica surfaces had the longest induction regime, implying the lowest friction between the sliding surfaces, when ethanol (fully spreading) was used as immersion fluid. A higher shear response (shorter induction zone) was measured with propanol (which correlated with weaker wetting by the liquid on the CTAB coated mica). The lubricating effect of LDPE surfaces modified with PE-*g*-PEO2000 when immersed in water (highest CA on CTAB) was worse even than in air when sheared against CTAB coated mica,

probably because of adhesion induced by the water at the hydrophobic CTAB surface. Isobutanol had the highest viscosity of all the investigated immersion fluids and its contact angle was higher than the one of ethanol and propanol. Isobutanol as immersion fluid showed an immediate response (no induction zone) when the LDPE surfaces modified with PE-*g*-PEO2000 were sheared against the CTAB coated mica surface. This is probably due to adhesion induced by the isobutanol at the hydrophobic CTAB surface.

## 6 Conclusions & Outlook

This thesis dealt with the investigation and characterisation of the effects on surface properties, especially friction, by introducing of linear and graft block copolymers into a homopolymer matrix film. The main findings of this thesis concern structural, morphological and lubricating properties. They can be summarised as follows:

- Careful studies on linear block copolymers of type PE-*b*-PEO incorporated into LDPE homopolymer suggested that micro-phase separated agglomerates were forming and no PEO was exposed at the LDPE surface, consistent with the observation of little change in the contact angle of water droplets on the surface. Incorporation of grafted block copolymer of type PE-*g*-PEO in LDPE films solvent-cast on a glass surface, on the other hand, revealed the presence of PEO at this LDPE surface via a reduction in the water contact angle.
- A Surface Force Balance was modified in such a way that shear responses were measurable between thick polymer films. This new technique—Shear Response Analysis (SRA)—was then used to measure the shear response of thick polymer films when sliding against mica and CTAB coated mica sheets. SRA could be used for high normal loads up to  $F_n = 25$  mN, corresponding to normal stresses of order  $\frac{25 * 10^{-3} N}{6.3 * 10^{-9} m^2} \approx 40$  atmospheres. This is comparable to pressures in mammalian joints (knees or hips).
- Sliding surfaces were investigated and their lubricating properties were measured up to these high normal stresses. The induction zones during compression (indicator for lubrication) were significantly enlarged by LDPE surfaces when modified by incorporation of PE-*g*-PEO, in good solvents for the PEO moieties.
- The higher the molecular weight of the side chain of the grafted block copolymer PE-*g*-PEO (two values were used), the better the lubricating effect in good solvents. The effect suggests that the grafted block copolymer forms a brush or a brush-like modifying PEO layer at the LDPE surface with the higher molecular weight PEO grafted chains apparently providing more efficient lubrication.
- In non-solvents for the PEO side chains, the PE-*g*-PEO did not act as lubricants. Good lubrication in a non-solvent was however provided in cases where the opposing surface coating was itself soluble in the immersion liquid. One can understand this effect as follows: PE-*g*-PEO modified LDPE in a non-solvent for the PEO behaved like a hard surface; when rubbed against mica, solid-solid friction resulted. However, when the mica was coated by CTAB which in the PEO non-solvent ethanol was itself

solvated, the effect was that of a solid (the modified LDPE) against a solvated or partially solvated “brush”, i.e. the CTAB layer itself, hence lower friction.

- Friction reducing surface modifications were not achieved by adding linear block copolymers to the LDPE matrix film but, as noted above, only by adding grafted block copolymer. Under thin film conditions, a morphology change could not be found by the introduction of grafted block copolymer as was the case with the introduction of linear block copolymers. The morphological change is expected to occur. Firstly, there is a micro-phase separation of the copolymer, then a macro-phase separation from the homopolymer to the block copolymer and finally an autophobic effect taking place at the interface between the homopolymer and the micro-phase separated block copolymer. Therefore, the assumption for the graft block copolymer is that few or no micro-phase separated agglomerates form and no autophobic effect of homopolymer avoiding the grafted block copolymer takes place.
- Block copolymer can be custom synthesised in order to avoid unfavourable structures formed by micro-phase separated block copolymer and enhance lubrication at polymer surfaces. Non-amorphous blocks of block copolymer may change their micro-phase separated structure according to the annealing history. Consequently, these architectures have to be controlled carefully in order to achieve the desired structures.

For further studies, several possibilities for investigations are imaginable. Since it is of considerable interest to achieve further insight into the lubricating properties under different solvent conditions, model systems could be used to investigate not only the good solvent conditions but also the  $\theta$ -solvent or bad solvent conditions. This could be achieved with a surface force balance for a more quantitative approach to the measurement of interacting surface forces. One such investigation could focus on asymmetric systems. For example, one side is a mica surface and the opposing sheet of mica is coated with either simple short-chained hydrocarbons like CTAB or with defined Langmuir-Blodgett deposited longer chained polymer. Self-assembled brush layer with well-characterised height in good solvent conditions would also be an interesting candidate for the opposing sheet of mica.

## 7 Bibliography

- 1 T. Ohta and M. Nonomura, *Elastic property of bilayer membrane in copolymer-homopolymer mixtures*. The European Physical Journal B **2**, 57-68 (1998).
- 2 G. Reiter, J. Schultz, P. Auroy, and L. Auvrav, *Improving adhesion via connector polymers to stabilize non-wetting liquid films*. Europhysics Letters **33**, 29-34 (1996).
- 3 D. A. Hajduk, H. Takenouchi, M. A. Hillmyer, F. S. Bates, M. E. Vigild, and K. Almdal, *Stability of the perforated layer (PL) Phase in diblock copolymer melts*. Macromolecules **30**, 3788-3795 (1997).
- 4 M. W. Matsen, *Stabilizing new morphologies by blending homopolymer with block copolymer*. Physical Review Letters **74**, 4225-4228 (1995).
- 5 G. H. Frederickson and F. S. Bates, *Stabilizing co-continuous polymer blend morphologies with ABC block copolymers*. The European Physical Journal B **1**, 71-76 (1998).
- 6 C. I. Yim, K. J. Kee, J. Y. Jho, and K. Choi, *Wear resistance of some modified ultra-high molecular weight polyethylenes and its correlation with tensile properties*. Polymer Bulletin **42**, 433-440 (1999).
- 7 V. Mangipudi, M. Tirrell, and A. V. Pocius, *Direct measurement of the surface energy of corona-treated polyethylene using the surface forces apparatus*. Langmuir **11**, 19-23 (1995).
- 8 L. Slusarski, D. M. Bielinski, S. Affrossman, and R. A. Pethrick, *Surface modification of elastomers to improve their tribological properties*. Elastomers and Plastics **51**, 429-438 (1998).
- 9 P. R. Lewis and C. W. McCutchen, *Mechanism of animal joints*. Nature **18**, 1284-1285 (1959).
- 10 C. W. McCutchen, *The frictional properties of animal joints*. Wear **5**, 1-17 (1962).
- 11 F. C. Linn, *Lubrication of animal Joints I. The arthrotripsometer*. The Journal of Bone and Joint Surgery **49-A**, 1079 (1967).
- 12 F. C. Linn, *Lubrication of animal joints II. The mechanism*. Journal of Biomechanics **1**, 193-205 (1968).
- 13 E. L. Radin, I. L. Paul, and P. A. Weisser, *Joint lubrication with artificial lubricants*. Arthritis and Rheumatism **14**, 126-129 (1971).
- 14 *Biomechanics: Mechanical properties of living tissue; Vol. ,* edited by Y. C. Fung (Springer Verlag, New York, 1993).

- 15 E. Kumacheva and J. Klein, *Simple liquids confined to molecularly thin layers. II: Shear and frictional behaviour of solidified films*. Journal of Chemical Physics **108**, 7010-7022 (1998).
- 16 J. Klein and E. Kumacheva, *Simple liquids confined to molecularly thin layers. I: Confinement-induced liquid-to-solid phase transitions*. Journal of Chemical Physics **108**, 6996-7009 (1998).
- 17 J. Klein, *Shear of liquid films confined to molecular dimensions*. Journal of Non-Crystalline Solids **235**, 422-427 (1998).
- 18 J. Klein and E. Kumacheva, *Liquid-to-solid transitions in thin liquid films induced by confinement*. Physica A **249**, 206-215 (1998).
- 19 J. Klein, in *Mechanism of friction across molecularly confined films of simple liquids*, 2000 (Elsevier (Amsterdam)).
- 20 J. Klein, Y. Kamiyama, H. Yoshizawa, J. N. Israelachvili, G. H. Fredrickson, P. Pincus, and L. J. Fetters, *Lubrication forces between surfaces bearing polymer brushes*. Macromolecules **26**, 5552-5560 (1993).
- 21 J. Klein, E. Kumacheva, D. Perahia, D. Mahalu, and S. Warburg, *Interfacial sliding of polymer-bearing surfaces*. Faraday Discussions **98**, 173-188 (1994).
- 22 J. Klein, *Shear of polymer brushes*. Colloids and Surfaces A: Physiochemical and Engineering Aspects **86**, 63-76 (1994).
- 23 J. Klein, E. Kumacheva, D. Mahalu, and D. Perahia, *Direct measurement of shear forces between polymer-bearing surfaces sliding past each other*. Macromolecular Symposia **98**, 1149-1158 (1995).
- 24 J. Klein, *Shear, friction, and lubrication forces between polymer-bearing surfaces*. Annual Reviews of Material Sciences **26**, 581-612 (1996).
- 25 J. Klein, in *Fundamentals of Tribology and Bridging the Gap between the Macro- and Micro/Nanoscales*, edited by B. Bhushan (Kluwer Academic Publishers, Printed in the Netherlands, 2001), p. 177-198.
- 26 M. Kernick and C. Allen, *The sliding wear of UHMWPE against zirconia in saline containing proteins*. Wear **203-204**, 537-543 (1997).
- 27 C. G. Moran, I. M. Pinder, T. A. Less, and M. J. Midwinter, *Survivorship analysis of uncemented porous-coated anatomic knee replacement*. Journal of Bone Joint Surgery **74-B**, 9-17 (1992).
- 28 V. Saikko, *Wear of polyethylene acetabular cups against zirconia femoral heads studied with a hip joint simulator*. Wear **176**, 207-212 (1994).
- 29 U. Bayer and R. Stadler, *Synthesis and properties of amphiphilic bumbbell-shaped grafted block-copolymers. I. Anionic synthesis via a polyfunctional initiator*. Macromolecular Chemistry and Physics **195**, 2709-2722 (1994).
- 30 J. Allgaier, A. Poppe, L. Willner, and D. Richter, *Synthesis and characterization of poly[1,4-isoprene-*b*-(ethylene oxide)] and poly[ethylene-co-propylene-*b*-(ethylene oxide)] block copolymer*. Macromolecules **30**, 1582-1586 (1997).

- 31 S. Förster and E. Krämer, *Synthesis of PB-PEO and PI-PEO block copolymers with alkylolithium initiators and the phosphazene base t-BuP4*. *Macromolecules* **32**, 2783-2785 (1999).
- 32 Å. Halldén and B. Wesslén, *Preparation and characterization of poly(ethylene-graft-ethylene oxide)*. *Journal of Applied Polymer Science* **60**, 2495-2501 (1996).
- 33 F. Scheffold, E. Eiser, A. Budkowski, U. Steiner, and J. Klein, *Surface phase behavior in binary polymer mixtures. I. Miscibility, phase coexistence, and interactions in polyolefin blends*. *Journal of Chemical Physics* **104**, 8786-8794 (1996).
- 34 M. L. Gee and J. N. Israelachvili, *Interactions of surfactant monolayers across hydrocarbon liquids*. *Journal of the Chemical Society: Faraday Transactions* **86**, 4049-4058 (1990).
- 35 H. N. Patrick, G. G. Warr, S. Manne, and I. A. Aksay, *Surface micellization patterns of quaternary ammonium surfactants on mica*. *Langmuir* **15**, 1685-1692 (1999).
- 36 R. Sterthaus, Thesis, MPI, 2001.
- 37 U. K. Chaturvedi, U. Steiner, O. Zak, and G. Krausch, *Interfacial structure in polymer mixtures below the critical point*. *Physical Review Letters* **63**, 616-619 (1989).
- 38 U. K. Chaturvedi, U. Steiner, O. Zak, G. Krausch, G. Schatz, and J. Klein, *Structure at polymer interfaces determined by high-resolution nuclear reaction analysis*. *Applied Physics Letters* **56**, 1228-1230 (1990).
- 39 G. Schatz and A. Weidinger, *Nukleare Festkörperphysik/Nuclear solid state physics* (B. G. Teubner, Stuttgart, Germany, 1992).
- 40 W. E. Kunz, *Deuterium  $^3\text{He}$  reaction*. *Physical Review* **97**, 456-462 (1955).
- 41 W. Möller and F. Besenbacher, *A note on the  $^3\text{He}+D$  nuclear reaction cross section*. *Nuclear Instruments and Methods* **168**, 111-114 (1980).
- 42 J. F. Ziegler, *The stopping and ranges of ions in matter*, Vol. 4 (Pergamon Press, New York, 1977).
- 43 J. F. Ziegler, *Handbook of stopping cross-sections for energetic ions in all elements* (Pergamon Press, New York, 1980).
- 44 J. F. Ziegler, J. P. Biersack, and U. Littmark, *The stopping and range of ions in solids* (Pergamon Press, New Yourk, 1985).
- 45 J. F. Ziegler and J. M. Manoyan, *Nuclear Instruments and Methods B* **35**, 215 (1988).
- 46 D. Schwahn, *Kleinwinkelstreuung und Reflexion mit Neutronen*. *Neutronenpraktikum Forschungszentrum Jülich* (1999).
- 47 L. Leibler, *Theory of microphase separation in block copolymers*. *Macromolecules* **13**, 1602-1617 (1980).
- 48 M. W. Matsen and F. S. Bates, *Unifying weak- and strong-segregation block copolymer theories*. *Macromolecules* **29**, 1091-1098 (1996).

- 49 T. Hashimoto, T. Kawamura, M. Harada, and H. Tanaka, *Small-angle scattering from hexagonally packed cylindrical particles with paracrystalline distortion*. *Macromolecules* **27**, 3063-3072 (1994).
- 50 H. Tanaka and T. Hashimoto, *Ordered structures of block polymer/homopolymer mixtures. 3. Temperature dependence*. *Macromolecules* **24**, 5713-5720 (1991).
- 51 D. Yamaguchi, T. Hashimoto, N. Y. Vaidya, and C. D. Han, *Effect of annealing on the perfection of ordered structure of highly asymmetric diblock copolymer*. *Macromolecules* **32**, 7696-7699 (1999).
- 52 L. Leibler and A. Ajdari, in *Wetting of grafted polymer surfaces by compatible chains*, Osaka, Japan, 1993.
- 53 *Wetting of grafted polymer surfaces by compatible chains; Vol. ,* edited by L. Leibler, A. Ajdari, A. Mourran, G. Coulon, and D. Chatenay (Springer-Verlag, Berlin, 1994).
- 54 L. Leibler and A. Mourran, *Wetting on grafted polymer films*. *MRS Bulletin January*, 33-37 (1997).
- 55 P. G. Ferreira, A. Ajdari, and L. Leibler, *Scaling law for entropic effects at interfaces between grafted layers and polymer melts*. *Macromolecules* **31**, 3994-4003 (1998).
- 56 K. Shull, *Wetting autophobicity of polymer melts*. *Faraday Discussions* **84**, 203-217 (1994).
- 57 K. Binder, in *Advances in Polymer Science; Vol. 112*, edited by P. H.-H. Kausch (1994), p. 181-299.
- 58 S. Ciccariello, J.-M. Schneider, B. Schönfeld, and G. Kostorz, *Generalization of Porod's law of small-angle scattering to anisotropic samples*. *Europhysics Letters* **50**, 601-607 (2000).
- 59 I. W. Hamley, (Oxford University Press, Oxford, 1998), p. chapter six.
- 60 I. W. Hamley, *Crystallization in block copolymers*. *Advances in Polymer Science* **148**, 113-137 (1999).
- 61 M. A. Hillmyer, W. W. Maurer, T. P. Lodge, F. S. Bates, and K. Almdal, *Model bicontinuous microemulsions in ternary homopolymer/block copolymer blends*. *Journal of Physical Chemistry B* **103**, 4814-4824 (1999).
- 62 S. T. Milner, *Polymer brushes*. *Science* **251**, 905-914 (1991).
- 63 H. J. Taunton, C. Toprakcioglu, L. J. Fetters, and J. Klein, *Forces between surfaces bearing terminally anchored chains in good solvents*. *Nature* **332**, 712-714 (1988).
- 64 J. Klein, D. Perahia, and S. Warburg, *Forces between polymer-bearing surfaces undergoing shear*. *Nature* **352**, 143-145 (1991).
- 65 R. Levicky, N. Koneripalli, M. Tirrel, and S. K. Satija, *Concentration profiles in densely tethered polymer brushes*. *Macromolecules* **31**, 3731-3734 (1998).
- 66 G. S. Grest, *Normal and shear forces between polymer brushes*. *Advances in Polymer Science* **138**, 149-183 (1999).

- 67 P.-Y. Lai and K. Binder, *Grafted polymer layers under variable solvent conditions: A Monte-Carlo simulation*. *Macromolecular Chemistry, Macromolecular Symposium* **65**, 189-198 (1993).
- 68 P.-Y. Lai and K. Binder, *Structure and dynamics of grafted polymer layers: A Monte-Carlo simulation*. *Journal of Chemical Physics* **95**, 9288-9299 (1991).
- 69 P.-Y. Lai and K. Binder, *Structure and dynamics of polymer brushes near the theta-point: A Monte-Carlo simulation*. *Journal of Chemical Physics* **97**, 586-595 (1992).
- 70 P.-Y. Lai and K. Binder, *Grafted polymer layers under shear: A Monte Carlo simulation*. *Journal of Chemical Physics* **98**, 2366-2375 (1993).
- 71 J. Israelachvili, P. M. McGuiggan, and A. M. Homola, *Dynamic properties of molecularly thin liquid-films*. *Science* **240**, 189-191 (1988).
- 72 J. Klein and E. Kumacheva, *Confinement-induced phase transitions in simple liquids*. *Science* **269**, 816-819 (1995).
- 73 S. Granick, *Motions and relaxations of confined liquids*. *Science* **253**, 1374-1379 (1991).
- 74 U. Raviv, P. Laurat, and J. Klein, *Fluidity of water confined to subnanometre films*. *Letters to Nature* **413**, 51-54 (2001).
- 75 U. Raviv and J. Klein, *unpublished*. .
- 76 J. Klein, E. Kumacheva, D. Mahalu, D. Perahia, and L. J. Fetters, *Reduction of friction forces between solid surfaces bearing polymer brushes*. *Nature* **370**, 634-636 (1994).
- 77 J. Klein, E. Kumacheva, D. Perahia, and L. J. Fetters, *Shear forces between sliding surfaces coated with polymer brushes: The high friction regime*. *Acta Polymerica* **49**, 617-625 (1998).
- 78 S. Granick, A. L. Demirel, L. L. Cai, and J. Peanasky, *Soft matter in a tight spot: Nanorheology of confined liquids and block copolymers*. *Israel Journal of Chemistry* **35**, 75-84 (1995).



As often a thesis is not the work of just a single person, and therefore I want to acknowledge the people who mainly supported and influenced this thesis.

First of all, there are my two advisors Prof. Dr. Jacob Klein and Prof. Dr. Günter Schatz, who made my stay in Israel possible and supported me whenever they could, even over the great distances between Oxford—Rehovot and Konstanz—Rehovot. Prof. Klein I would like to thank that I had the chance to work in his group, where I always had the possibility to develop my ideas very freely and independently with his careful supervision and directing. Prof. Schatz I especially would like to thank because he not only observed my progress with the NRA but also made NRA again possible, after a long shut down where he had the right connections to suppliers at the right time.

I would like to thank Dr. Rachel Yerushalmi-Rosen. With her it was always a pleasure to discuss science and life in Israel in general. She also read my thesis draft and gave her opinion and helpful suggestions.

In the collaboration with the group of Prof. Dr. Dieter Richter (Forschungszentrum Jülich) I greatly acknowledge the help of Dr. Jürgen Allgaier for assisting in the synthesis of my working tool the linear block copolymer. Furthermore I would like to thank Dr. Dietmar Schwahn for measuring and discussing the SANS data.

Herut Sharan I would like to acknowledge as the great secretary and helpful “mother” of PostDocs, PhD-, Master-, and Diploma students. She made the life abroad a lot more pleasant and always had a “tip” which places are very beautiful to visit in Israel. Yehudit Rouso and Zelu Yzиковich I would like to thank for their great help and that they managed to supply me with all the necessary stuff I needed during my studies. Menashe Levi I would like to thank for his constant help against problems “with” and “within” the Perlman Building –from lockers to air conditioning– and his help to organise those little but desperately needed things.

Ygal Shachar I would like to thank for his outstanding and never ending motivation to maintain again and again the old Van de Graaff accelerator and therefore kept NRA alive. He also constantly improved the working conditions with and around the accelerator.

Tobias Kerle I would like to thank for lots of discussions not only about computer networks and science, but also about general topics. He became a very good friend during the time we spent together and it was always very nice to explore with him the hidden and interesting sites all over Israel.

I also would like to thank several students for very interesting discussions who became not only friends but also very prosperous scientists as there are Michael Wendlandt, Harald Hoppe and Rossen Apostolov.

The rest of Prof. Klein’s group I would like to thank as well for interesting discussions not only about science as there are Dr. Susan Rubin, Hila Moatti-Poupko, Dr. Xuean Zhang, Dr. Larisa Tsarkova, Uri Raviy, Rafi Tadmor and Christoph Schreiter. Daniel Frankel, I would like to acknowledge for reading and correcting the English phrasing of my thesis draft.

I would like to thank my parents and grandparents without their financial support it would not have been possible to study at all. In addition during my times abroad they had to deal with the bureaucracy in Germany and kept my accounts running. Furthermore they gave me the possibilities to develop and decide freely and independently and supported me in all my decisions.

I would like to thank Anke for keeping the contact and mental support also over thousands of kilometres and of course for the fun we had together exploring Israel and the easily accessible (from Israel) regions of the middle east.

The German Israel Foundation (GIF) I would like to thank for financing my PhD studies and some travel expenses to interesting conferences worldwide.

Last not least I would like to thank all the Israeli and friends from foreign countries, I met here in Israel and had fun with, outside the lab under non-studying circumstances.